Measurement report: Molecular Insights into Organic Aerosol Sources and Formation at a Regional Background Site in South China

Hongxing Jiang¹, Yuanghang Deng¹, Yunxi Huo¹, Fengwen Wang², Yingjun Chen³, Hai Guo^{1,4*}

¹Air Quality Studies, Department of Civil and Environmental Engineering, The Hong Kong Polytechnic University, Hong Kong, China

²Key Laboratory of the Three Gorges Reservoir Region's Eco-Environment, Ministry of Education, College of Environment and Ecology, Chongqing University, Chongqing, 400030, China

³Shanghai Key Laboratory of Atmospheric Particle Pollution and Prevention (LAP³), Department of Environmental Science and Engineering, Fudan University, Shanghai 200433, China

⁴Research Institute for Land and Space, The Hong Kong Polytechnic University, Hong Kong, China

Correspondence to: H. Guo (hai.guo@polyu.edu.hk)

Abstract. Understanding their chemical composition and quantifying the sources of organic aerosols (OA) are crucial for assessing their formation and human-related effects, yet individual mass spectrometry techniques still struggle to reveal the effects of sources and atmospheric processes on OA composition at the molecular levelbut still face challenges. In this 15 study, we combined for the first time a high-resolution time-of-flight aerosol mass spectrometer (AMS), a thermal-desorption aerosol gas-chromatograph-mass spectrometer (TAG-MS), and an electrospray ionization high-resolution orbitrap mass spectrometer (HR-MS) to analyze OA at a background site in South China from bulk to molecular levelswe examined OA at a background site in South China, analyzing from bulk to molecular levels, utilizing a high-resolution time-of-flight aerosol mass spectrometer (AMS), a thermal desorption aerosol gas-chromatograph-mass spectrometer (TAG-MS), and an electrospray ionization high-resolution orbitrap mass spectrometer (HR-MS). Compared to our previous study, a pPositive matrix factorization (PMF) analysis based on AMS data and organic tracers from TAG-MS were applied to provide detailed source contributions of AMS components. We found showed that that biomass burning-related OA and gas-phase secondary OA (gas pSOA) were the primary sources of the low-oxidized oxygenated OA (LO-OOA1) was mainly contributed by biomass burning-related OA (BB-OA) and gas-phase secondary OA (gas-pSOA), while the high-oxidization degree of more-oxidized oxygenated OA (MO-OOA) was mainly due to isoprene-derived secondary OA. Oxidation processes significantly increased the accumulation of CHO compounds, and human-biological interactions enhanced the diversity of CHON compounds. Using a constrained non-negative matrix factorization (NMF) approach constrained by PMF source contributions on to offline HR-MS data, we identified we found that while CHO compounds dominated the molecules associated with each sourcePMFresolved factor, the degree of oxidation and unsaturation varied significantly among them. Specifically, tThe NMF resolved cooking-related OA (C-OANME) factor exhibited the highest O/C ratio but the lowest double bond equivalent (DBE) value, whereas the BB-OA_{NMF} factor was characterized by the greatest aromaticity and a high abundance of nitroaromatics. For secondary processes, sulfur additions played a more significant role in gas-pSOA than in secondary inorganic aerosol-related OA Is (SIA-OA). Overall, this study enhances our understanding of the sources and formation of different AMS components,

设置了格式: 字体: (默认) Times New Roman

设置了格式: 上标

设置了格式: 上标

设置了格式: 字体: (中文) +中文正文(宋体), (中文) 简体中文(中国大陆)

设置了格式: 字体: Times New Roman

设置了格式: 下标

设置了格式: 非上标/下标

设置了格式: 下标

设置了格式: 字体: 倾斜

reveals the impact of different sources on the molecular composition of OA, and our results underscore the prominent impact of anthropogenic emissions and their photo-oxidation on ambient OA in areas with low PM particulate matter pollution but high O₃ levels.

1 Introduction

Organic aerosols (OAs), which make up 20%-90% of fine particulate matter (Jimenez et al., 2009; Kanakidou et al., 2005), have garnered significant scientific interest due to their substantial climate forcing (Mahowald, 2011; Szopa et al., 2021), environmental impacts, and health effects (Daellenbach et al., 2020). These aerosols are complex mixtures influenced by primary emissions from both anthropogenic and biogenic sources, as well as secondary chemical processes involving volatile organic compounds (VOCs) through multiphase atmospheric reactions (Ziemann and Atkinson, 2012). Understanding the chemical composition, origins, and formation mechanisms of OA is crucial for assessing their adverse effects and developing effective control strategies. However, the chemical complexity of OA, characterized by diverse functional groups and molecular structures, presents significant analytical challenges (Jimenez et al., 2009). In recent decades, there have been remarkable advancements in analytical techniques, evolving from traditional offline gas/liquid chromatography-mass spectrometry (GC/LC-MS) methods that identify limited tracer compounds to state-of-the-art online instruments like extractive electrospray ionization (EESI-TOF-MS) and chemical ionization time-of-flight mass spectrometer (CI-TOF-MS), which enable near-molecular real-time measurements (Ervens et al., 2024). High-resolution mass spectrometry (HR-MS), including orbitrap and Fourier transform ion cyclotron resonance mass spectrometers, has become widely used for characterizing chemical composition of OA at molecular level. These techniques facilitate the detection of thousands of molecular species, significantly enhancing our understanding of OA composition (Noziere et al., 2015; Laskin et al., 2018).

Current methodologies for source apportionment of OA primarily employ receptor models such as positive matrix factorization (PMF). These approaches include: (1) tracer-based PMF, which relies on a limited set of molecular markers (Reff et al., 2007), and (2) coupling aerosol mass spectrometry (AMS)-based chemical composition with PMF (Jimenez et al., 2009; Ulbrich et al., 2009). The tracer-based PMF often identifies ambiguous SOA factors (e.g., secondary inorganic aerosols) with uncertain chemical mechanisms and source contributions (Reff et al., 2007; Wang et al., 2017a; Lyu et al., 2020). Although AMS-PMF has successfully resolved specific OA sources, i.e., biomass burning and cooking, in certain regions (Zhou et al., 2020), it faces limitations in achieving chemical specificity for OA from many other important sources. (Zhang et al., 2018) Typically, AMS-PMF categorizes the predominant OA mass fraction based on oxidative characteristics rather than specific emission sources, i.e., low-oxidized and more-oxidized oxygenated OA (Zhou et al., 2020; Zhang et al., 2018). Emerging techniques like EESI-TOF-MS now allow for near-molecular online measurements (Lopez-Hilfiker et al., 2019), and when coupled with advanced statistical methods such as bin PMF, they can explore the components and sources of OA (Zhang et al., 2019; Nie et al., 2022). However, challenges remain in offline HR-MS-based source apportionment due to the lack of structural information for identified compounds, and the detection of more compounds compared to online TOF-MS. Different

structural isomers from biogenic VOCs (BVOC) and anthropogenic aromatics often share identical molecular formulas, complicating molecule-level source apportionments (Zheng et al., 2023).

To address these questions, we conducted a comprehensive study on the composition and sources of OA at a regional background site in Hong Kong during September-November 2020, a period marked by global lockdowns due to the COVID-19 outbreak. Advanced analytical techniques including high-resolution AMS (HR-AMS), thermal-desorption aerosol gaschromatography coupled with time-of-flight mass spectrometry (TAG-TOF-MS), and high-performance liquid chromatography with high-resolution mass spectrometry (HPLC-HR-MS) were utilized in the study. Although the composition, origin, and evolution of OA in Hong Kong have been extensively studied, previous research primarily relied on HR-AMS measurements and analyses based on molecular markers (Li et al., 2013b; Qin et al., 2016; Lyu et al., 2020; Huo et al., 2024a). Given that OA in Hong Kong is influenced not only by local emissions, i.e., vehicle exhaust and cooking, but also by regional transport (Lyu et al., 2020; Huo et al., 2024b), the complex interactions of these sources necessitate a deeper understanding of OA composition and sources at the molecular level.

2 Experimental methods

80

2.1 Sampling campaign and online measurements

A comprehensive sampling campaign was conducted at the regional background site Hok Tsui (HT, 22.20° N, 114.253° E) from September 29 to November 18, 2020. This site is situated on the southeastern tip of Hong Kong Island, facing the South China Sea. During the campaign, 31 valid daily fine particulate matter (PM_{2.5}) samples were collected from November 7 to November 16, 2020, using a high-volume sampler (TE-6070, TISCH, U.S) operating at a flow rate of approximately 1.0 m³·min⁻¹ (Table S1). Prebaked quartz filters (450°C for 5h) were used to capture the particle matter, and the filters were subsequently wrapped in pre-baked aluminum foil after sampling. Field blank samples were also collected to ensure data accuracy. All samples were transported to the laboratory and stored at -20 °C prior to analysis.

A suite of online instruments was utilized to simultaneously measure gaseous pollutants and the chemical composition of particulate matter. To align with the PM_{2.5} sampling periods, the online datasets were filtered for use in this study. HR-TOF-AMS was used to measure the composition of non-refractory submicron particulate matter (PM₁). Using Combing with the PMF method, four OA components were identified: a hydrocarbon-like OA (HOA), two less-oxidized oxygenated OAs (LO-OOA1 and LO-OOA2), and a more-oxidized oxygenated OA (MO-OOA) (Figure S1). Additionally, a TAG-TOF-MS was employed to measure organic markers, while a Proton Transfer Reaction time-of-flight mass spectrometer (PTR-TOF-MS) was applied to determine ambient concentrations of VOCs. Detailed information on the instrumental settings, calibrations, and data processing for HR-TOF-AMS (Huo et al., 2024a; Yao et al., 2022). (Huo et al., 2024a; Yao et al., 2022), TAG-TOF-MS (Huo et al., 2024b; Lyu et al., 2020), and PTR-TOF-MS (Yuan et al., 2024; Lyu et al., 2024) can be found in previous studies and is also briefly described in Supplementary text and Table S2. Furthermore, concentrations of PM_{2.5}, a series of trace gases (CO, NO, NO₂, O₃ and SO₂), and meteorological parameters (temperature, relative humidity) were continuously monitored.

2.2 HPLC-HR-MS analysis

100

105

110

115

120

The molecular composition of OAs in the offline $PM_{2.5}$ filters was analyzed using a high-resolution Q-Exactive Orbitrap mass spectrometer (Thermo Electron, Inc.) equipped with a heated electrospray ionization (ESI) source operating in negative mode. To address potential intermolecular suppression effects during ionization, an ultra-high performance liquid chromatography system (UHPLC, Dionex UltiMate 3,000, Thermo Electron, Inc.) was employed for compound separation_shighlighting possible challenges (Zhang et al., 2024; Thoma et al., 2022). Detailed descriptions of the analysis procedures and instrumental settings are available in Supplementary text (Zhang et al., 2024; Wang et al., 2017b). Briefly, two pieces of $PM_{2.5}$ filters were punched using a stainless-steel puncher (Φ =20 mm), and the dissolved organic matter was extracted with 6 mL of mix-solvents (2×3 times, methanol: toluene=1:1, v/v) using an ultrasonic cold-water bath for 20 minutes. The extracts were filtered through a 0.22 µm polytetrafluoroethylene membrane, combined, and evaporated to near dryness under a gentle stream of high-purity nitrogen. The residue was redissolved in 150 µL of methanol and centrifuged, with the supernatant transferred for subsequent HR-MS analysis. The scanning range of m/z was set from 50 to 800, with a typical mass resolution of 140 000 at m/z 200.

Non-target compound analysis was performed using the open-source software MZmine-2.37 (http://mzmine.github.io). The analysis workflow included raw data import, peak detection, shoulder peak filtering, chromatogram building, chromatogram deconvolution, deisotoping, searching for adducts and peak complexes, alignment, gap filling, identification, and duplicate peak filtering (Wang et al., 2017b). Mass peaks were assigned to specific molecules with a mass tolerance of 2 ppm for ESI- mode. The molecular formulas were constrained to $C_{1-40}H_{0-100}O_{0-40}N_{0-5}S_{0-3}$, with additional criteria applied to elemental ratios (e.g., H/C, O/C) and double bond equivalents (DBE) to exclude chemically implausible formulas (Wang et al., 2017b; Lin et al., 2012). Elemental ratios, DBE, and modified aromatic index were calculated based on the assigned formulas of $C_cH_hO_oN_nS_s$, where c, h, o, n, and s are the number of carbon, hydrogen, oxygen, nitrogen and sulfur atoms, respectively. All reported molecules underwent blank subtraction, and those with an abundance ratio of less than 5:1 were excluded from the study (Ditto et al., 2018).

2.3 Positive matrix factorization (PMF)

The EPA PMF5.0 model was employed to determine the relative contributions of different sources to the four AMS-PMF OAs. The mathematical framework of PMF has been described in detail in previous studies (Hopke, 2016; Norris et al., 2014). In brief, we used hourly concentration data of AMS-PMF OAs and SOA tracers as input for the EPA PMF model. While incorporating total OA mass along with chemical tracers in the PMF analysis can help distinguish the contributions of different sources to OA, it does not provide detailed source information for these AMS components, nor does it reveal how atmospheric conditions influence their oxidation states. The uncertainty $u_{i,j}$ for each species was calculated using the following equations:

$$u_{i,j} = (\mathbf{x}_{i,j} \times \text{error fraction} + (0.5 \times \text{MDL})^2)^{1/2} (\mathbf{x}_{i,j} \ge \text{MDLs})$$

$$u_{i,j} = 5/6 \times MDL (x_{i,j} \ge MDLs)$$

where x_{i,j} denotes the concentration of species *i* in sample *j*, and MDLs is the method detection limits for each species. Given that the concentrations of species used in PMF analysis can vary by orders of magnitude, applying the default error fraction may lead PMF to treat high concentration data as outliers, thereby reducing model robustness and increasing uncertainty in the results (Wang et al., 2017a). To address this issue, we adopted the error fraction of 0.2 for OA components and polar SOA tracers, and 0.3 for n-alkanes (Wang et al., 2019). The PMF model decomposes the x_{i,j} matrix into factor profile (f_{k,j}) and
contribution matrices (g_{i,k}) by minimizing the scaled residue (Q) based on the u_{i,j} matrix. The optimal number of factors were preliminarily determined by examining the change in Q_{ture}/Q_{exp} from 2-10 factors (Figure S2). Bootstrapping (BS) was then applied to test the robustness of each solution, with factor matching rates above 80 % considered acceptable (Jiang et al., 2024). Ultimately, a six-factor solution was adopted, which showed good correlations between modeled and measured concentrations of each AMS-PMF derived OA component (r = 0.70-0.94), supporting the validity of using AMS-components as input variables.

2.4 Non-negative matrix factorization (NMF)

150

155

160

The mathematical frameworks of PMF and NMF are virtually identical, with the key difference being that NMF only requires input values to be non-negative. Additionally, the error matrix required for EPA PMF analysis is typically unnecessary for NMF. These characteristics make NMF particularly suitable for factor decomposition of HR-MS data, where determining the detection uncertainty for each molecule is often challenging. (Rund et al., 2023) (Rund et al., 2023). The NMF routine was applied to the molecular composition data from the offline filter samples. However, we observed that compared to previous online TOF-MS analyses, the number of identified molecules using HR-orbitrap-MS increased significantly, reaching thousands, with some compounds sharing the same formulas but potentially having multiple sources. This complexity poses significant challenges for the interpretability of NMF factors. To address this, daily concentration data for the six factors obtained from the tracer-based PMF model were also used as constraints in the NMF model. This approach not only enhances the interpretability of NMF factors but also helps elucidate the molecular formation mechanisms underlying the PMF factors. Specifically, the contribution matrix of PMF factors was combined with the intensity-normalized data of HR-MS molecules to form a comprehensive input matrix, X.

$$X \sim G \times F$$

The NMF analysis was conducted using a R package "NNLM," which tests the performance of 2–10 factors. The function of "nnmf" decomposes the input matrix X into two non-negative matrices, G and F, by minimizing the root-mean squared residual (RMSE) between X and its approximation, GF. Through this approach, both the percentages of PMF factors contributing to each NMF factor and the intensity fraction of each NMF factor relative to the total molecular intensity can be derived from the reconstructed matrix of GF. To determine the optimal number of factors, we plotted the variation of RMSE against the number of factors and selected the optimal value based on the Elbow rule (i.e., the point at which the RMSE reaches a minimum). We also calculated the global relevance between X and GF, following the method described by Rund et al. (2023),

to identify the number of factors that best explain the variance. Furthermore, consensus cluster analysis was performed using the R package "ConsensusClusterPlus" (Monti et al., 2003) to further support the selection of the appropriate number of factors. By integrating all these evaluation criteria, we determined that five-factor was the optimal choice, as this was the smallest number that explained 99% of the variance in the input data matrix (Figure S3). It is noteworthy that the modeled factor concentrations showed good correlations with the input values, with average uncertainties ranging from 0.1% to 1.5%.

2.5 Trajectory Cluster Analysis

165

185

To assess the potential influences of regional transport on the composition of OAs during the sampling campaign, we used the National Oceanic and Atmospheric Administration (NOAA) Hybrid Single Particle Lagrangian Integrated Trajectory (HYSPLIT) model (https://www.ready.noaa. gov/HYSPLIT.php) to calculate 120-h backward trajectories at 100 m heights using archived Global Data Assimilation System meteorological data (ftp://arlftp.arlhq. noaa.gov/ pub/archives/reanalysis). These hourly trajectories were clustered into three categories (C1-C3, Figure S4) based on their origins and transport pathways. Category C3 (41%) consisted of short-range continental air masses originating from central and northern China, reaching Hong Kong after traversing the Pearl River Delta (PRD) region. Category C2 (37%) originated from North China and arrived in Hong Kong after passing through the East China Sea and coastal cities in southern China. The origins of Category C1 (22%) could be traced to Mongolia, with air masses transported to Hong Kong along eastern and southern coastal cities. Additionally, a potential source contribution function (PSCF) analysis was conducted to evaluate possible source regions of PMF-derived source factors. (Jiang et al., 2024) (Jiang et al., 2024). The PSCF analysis was performed using the open software MeteoInfo, with the 50th percentile of OA concentrations set as the threshold for PSCF calculations.

180 3 Results and discussion

3.1 OA composition and influencing factors

It should be noted that although our previous study (Huo et al., 2024a) reported AMS results, the differing time windows between the two studies may lead to different conclusions. To ensure consistency with the offline $PM_{2.5}$ samples analyzed in this study, only the AMS data corresponding to the same sampling period were selected and reanalyzed. Notably, even though the sampling campaign occurred during a period influenced by both continental and costal air masses from mainland China, the observed $PM_{2.5}$ concentrations remained relatively low (11-35 μ g·m³, mean:18 \pm 5.0 μ g·m³). This level was notably lower than historical urban measurements in Hong Kong (Wu et al., 2018). Yet, it still substantially exceeded the WHO guideline of 5 μ g·m³. The reduction in $PM_{2.5}$ concentrations could be attributed to decreased anthropogenic emissions during the COVID-19 lockdown period (Huo et al., 2024a). Organic matter (OM=1.8×OC) (Gao et al., 2016) constituted 34 \pm 16% of the $PM_{2.5}$ mass, with its fractional contribution increasing to 52 \pm 5.1% in PM_{1} , as quantified by AMS (Figure 1a), underscoring the critical role of OA in particulate matter formation. In our previous study, four OA components were identified in PM_{1} using the AMS-PMF method throughout the sampling period, including one HOA and three OOA factors (Huo et al., 2024a). As

设置了格式: 下标

shown in Figure 1a, the temporal variation of OA concentrations was predominantly driven by LO-OOA1 (44 ± 12%) and MO-OOA (32±9.7%), both influenced by regional transport, particularly LO-OOA1. For example, the highest OA 195 concentrations were observed on the evening of November 6th, influenced by C3 air masses from central/northern China, with LO-OOA1 contributing up to ~70% of the OA, indicating regional transport as a potential driver of OA variation. For MO-OOA, back trajectory analysis revealed that air masses originating from continental China (C3) were associated with ~17% enhancements in MO-OOA concentrations (Figure S4b). In contrast, HOA and LO-OOA2 exhibited limited temporal variation (each comprising ~12% of total OA) and varied less across air mass clusters, reinforcing their characterization as background OA components at this site. Our previous investigation identified photochemical processing as the dominant formation pathway for LO-OOA1 and MO-OOA compared to aqueous-phase reactions throughout the whole sampling period, evidenced by their differential correlation responses to oxidant levels and relative humidity (Huo et al., 2024a). In addition, photochemical reactions involving anthropogenic emissions have been shown to play a particularly important role in the formation of LO-OOA1, whereas MO-OOA is more influenced by biogenic emissions. However, dDuring the focused sampling period in this study, LO-OOA1 exhibited strong associations with gas-phase photochemical reactions involving both biogenic and anthropogenic VOCs species, as well as NOx (Figure S5). In contrast, MO-OOA was more closely associated with SOA formation processes driven by ozone oxidation of BVOCs, as evidenced by strong correlations between MO-OOA and both O₃ and biogenic SOA tracers (r>0.50, p<0.01). For another OA component, LO-OOA2, only a limited number of species (e.g., hydroxyglutaric acids and adipic acid) showed good correlations with its concentrations, suggesting distinct secondary processes in its formation. Strong correlations were observed between HOA and anthropogenic species related to primary emissions, such as toluene, Benzenebenzene/ethylbenzene fragments, NO_k and high-molecular-weight alkanes (>C₂₅). HOA was generally considered to relate to vehicle emissions. While vehicle emissions are important sources of benzene-like species and NO_x (Yuan et al., 2024), they predominantly emit low-molecular-weight alkanes (<C₂₆) (Geng et al., 2019; Fu et al., 2011). The high-molecular-weight alkanes are mainly derived from higher plants, but particles from primary biological emissions are 215 typically in the coarse mode (Fu et al., 2011). Thus, our results suggest that HOA might also be influenced by anthropogenic emissions associated with biogenic materials, such as biomass burning or cooking. The presence of m/z 55, 57 and CO₂⁺ in the mass spectra of HOA supports these speculations (Zhou et al., 2020).

设置了格式: 下标

设置了格式: 下标

设置了格式: 下标

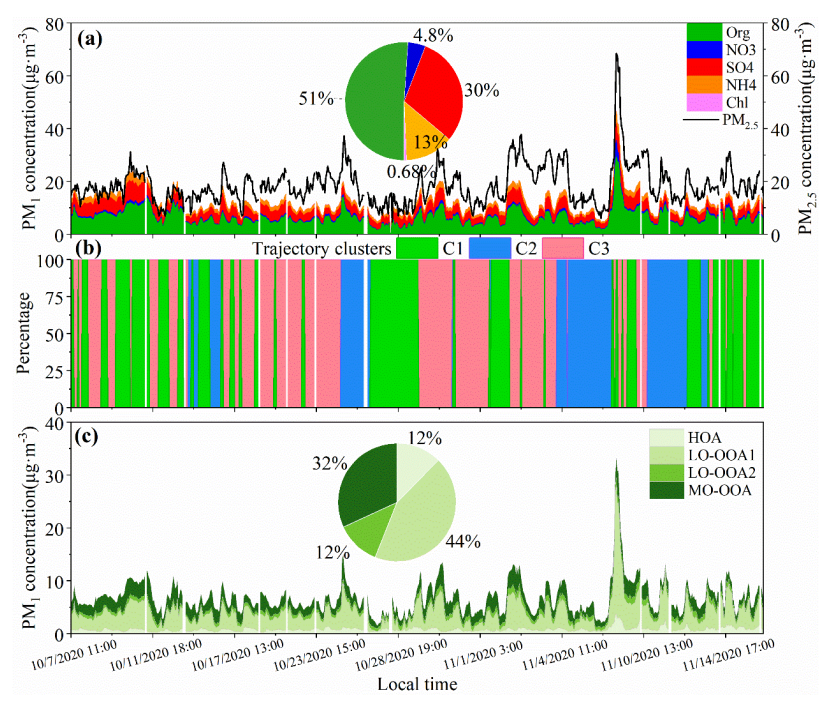


Figure 1: (a) Temporal variations in the mass concentrations of AMS-PM₁ components and PM_{2.5}. The pie chart illustrates the 220 average proportions of each species contributing to the total PM₁. (b) Air mass clusters based on 120-hr backward trajectories arriving at the sampling site during the study period. (c) Temporal variations in the mass concentrations and average proportions of AMS-PMF derived OA components.

3.2 Source contributions and origins of OA

To elucidate source-specific contributions to AMS-resolved OA components, we performed PMF analysis by integrating AMS-OA components, SOA tracers from TAG-TOF-MS, and VOC data from PTR-TOF-MS. Despite differences in particle cut-off sizes between AMS and TAG-TOF-MS, the AMS-derived OA mass was 110% (62-230%) of the OC/EC-based estimation in PM_{2.5}, confirming substantial organic matter enrichment in PM₁. The positive correlation between the results obtained from these two methods further supports the integration of the datasets (Figure S6, r=0.54, p<0.01). This combined approach has been successfully applied in several previous studies to determine OA sources (Huo et al., 2024a; Huang et al., 2021). Based on the chemical species loading in each factor, we tentatively attributed the PMF-derived six factors to biomass burning related OA (BB-OA), cooking-related OA (C-OA), isoprene-derived SOA (Iso-SOA), monoterpene-derived SOA

(MT-SOA), secondary inorganic aerosol-related OA (SIA-OA), and gas-phase photochemical SOA (gas-pSOA), respectively (Figure S7). Figure 2c-i also presents the diurnal variations of OA concentrations contributed by each PMF factor.

The BB-OA and C-OA factors were predominantly composed of levoglucosan isomers (Simoneit, 2002) and oleic acid (Rogge et al., 1991), respectively. The OA concentrations from these factors exhibited similar diurnal patterns, peaking in the morning, declining during the daytime, and rising again in the evening (Figure 2c-d). Notably, the C-OA factor also demonstrated high loadings of toluene and C8 aromatics, consistent with previous studies indicating that cooking processes can emit significant fractions of aromatic compounds formed through the cyclization of unsaturated fatty acids (Song et al., 2022; Song et al., 2023). The two biogenic SOA factors, Iso-SOA and MT-SOA, were characterized by high loadings of 2methylglyceric acid and C5-alkenetriols for Iso-SOA, and 3-methyl-1,2,3-butanetricarboxylic acid and Pinic acid for MT-SOA (Li et al., 2013a; Ding et al., 2016). The diurnal variations of OA contributed by these factors showed distinct patterns, with Iso-SOA peaking in the afternoon (14:00-15:00) and MT-SOA reaching its highest values at noon, suggesting differences in their formation mechanisms. Comparisons with the diurnal variations of NO2, O3, and jNO2 (the photolysis frequency of NO₂) suggest that Iso-SOA may be related to O₃ oxidation, whereas MT-SOA is associated with NO₂ photocatalytic oxidation. Both factors showed positive correlations with temperature (r > 0.50, p < 0.01), consistent with previous studies indicating that elevated temperatures can enhance the emission of biogenic VOCs (Ding et al., 2016; Ding et al., 2011). The gas-pSOA factor exhibited high loadings of VOCs species, including photochemical products from both biogenic and anthropogenic species, supporting its association with gas-phase photochemical processes. This factor was less abundant in particle-phase SOA tracers, implying that gas-pSOA would produce less-oxidized or first-generation SOA products. The synchronous diurnal variation of gas-pSOA-contributed OA with O₃ suggested that gas-phase oxidation by O₃ was the main formation pathway, rather than oxidation by NO₂ photolysis (Figure 2). SIA-OA was characterized by high loadings of nitrates, sulfates, and ammonium, along with anthropogenic SOA tracers such as m-/o-phthalic acid, hydroxylated benzoic acids, and low-molecular-weight alkanes (<C₂₆), suggesting influences from anthropogenic emissions such as biomass burning and vehicle emissions (Fu et al., 2011). The SIA-OA showed low values at noon but increased in the afternoon, peaking at 20:00, with a diurnal pattern similar to RH but opposite to NO₂. As NO₂ photolysis weakens and RH increases, heterogeneous processes could promote the formation of SIA. Furthermore, nocturnal oxidation of VOCs initiated by the NO₃ radical and O₃ might be an important source of SIA-OA, as nighttime oxidation has been reported as a major pathway of SOA formation globally, particularly through NO₃· radical-initiated oxidation (Pye et al., 2010; Hoyle et al., 2007; Liu et al., 2024).

240

245

260

265

Figure 2a shows the time series of OA concentrations contributed by each factor. Overall, variations in OA concentrations during the sampling period were mainly associated with gas-pSOA, BB-OA, and SIA-OA, contributing 29%, 22%, and 20% to the total OA, respectively. Biogenic SOA-related processes and cooking-C-OA accounted for 18% and 11% of OA, respectively. Figure 2b illustrates the contributions of PMF factors to each AMS-OA component. For LO-OOA1 and MO-OOA, which were the two main components driving OA variations throughout the sampling period, different contributions from SOA factors were evident. The combined contributions of gas-pSOA and BB-OA to LO-OOA1 exceeded 70%, while SIA-OA's contribution was negligible. In contrast, the contribution of gas-pSOA to MO-OOA decreased to 21%, with SIA-

OA having the highest contribution to MO-OOA at 38%, followed by biogenic SOA processes (Iso-SOA: 22% and MT-SOA: 11%). Therefore, the relatively higher oxidation degree of MO-OOA compared to LO-OOA1 could be attributed to greater contributions from SIA-OA and/or biogenic SOA processes. However, given that LO-OOA2 has an even higher proportion of SIA-OA (46%) than MO-OOA, along with similar contributions from gas-pSOA, this suggests that the formation of highly oxidized organic compounds in MO-OOA might not be primarily driven by SIA-OA processes. Instead, it appeared to be more closely associated with biogenic SOA processes, particularly those involving Iso-SOA.



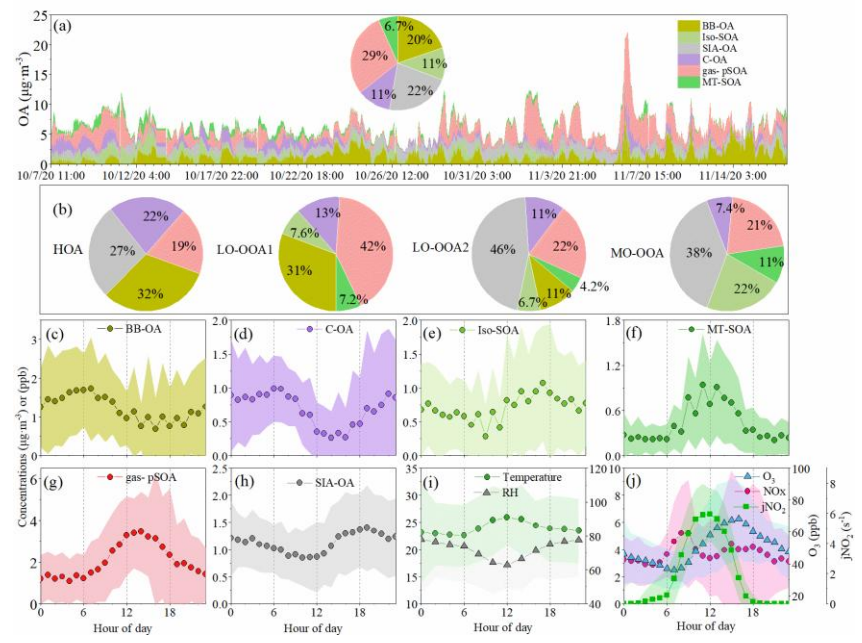


Figure 2: (a) Temporal variations in OA concentrations attributed to each PMF factor. The accompanying pie chart shows the average contribution of each PMF factor over the sampling period. (b) Average contributions of each PMF factor to the AMS-OA components. (c-h) Diurnal variations of OA concentrations contributed by each PMF factor, and (i-j) Diurnal variations in environmental conditions, including temperature (°C), RH (%), oxidant levels.

A PSCF analysis was conducted to identify the potential source regions for each OA factor obtained from the tracer-based PMF analysis during the sampling period. As shown in Figure S8, one of the major source regions for BB-OA was central-northern China, including Henan and Shanxi provinces, where straw burning was an important source of PM_{2.5} during the harvest season. Another source region for BB-OA was northern China and the Korean Peninsula, with fire maps (Figure S9)

设置了格式: 下标

indicating intense open BB activities in these regions during periods of elevated BB-OA. Southern China, including local emissions, was identified as a medium to high potential region for both biogenic SOA (IsopreneSOA—IsoOSOA and TerpeneSOAMT-SOA) and ecokingC-OA, due to high biogenic emissions and cooking contributions in these regions (Zhang et al., 2025; Yao et al., 2021). However, coastal regions, including northern China and the Korean Peninsula, were also potential source regions for Iso-SOA, indicating that combustion-related sources might also play a significant role (Zhang et al., 2025). For OA related to gas-pSOA and SIA-OA, the medium to high potential source regions for gas-pSOA were coastal cities in eastern and southern China. In contrast, the potential source regions for SIA-OA also included northwestern China, such as Shanxi and Shaanxi provinces, where these regions often experienced high NO_x and SIA-OA concentrations due to anthropogenic emissions, e.g., coal combustion (An et al., 2019).

0 3.3 Molecular composition of OA

285

300

The integration of molecular tracers with AMS analysis provides an effective approach for elucidating the sources of OA, emphasizing the significant role of SOA processes in OA formation in South China. However, the molecular transformation mechanisms underlying the PMF-resolved factors, particularly for SOA, remain unclear. Thus, the molecular composition of OA was analyzed using an ESI- HPLC-HRMS based on offline daily $PM_{2.5}$ samples collected during the sampling period. A total of 10,012 unique molecular formulas were identified across all samples, among which CHO compound accounted for 30 \pm 2.7% of formular number, but their relative intensity was $67 \pm 4.9\%$ (Figure 3a). Correspondingly, CHON compounds accounted for $42 \pm 6.1\%$ of the formular number, but their contribution to total intensity was only $15 \pm 3.2\%$. Additionally, the measured sulfur-containing organic compounds (CHOS+CHONS) accounted for $18 \pm 5.4\%$ of the total intensity. Unlike many studies conducted in mainland China, which are substantially influenced by anthropogenic emissions or liquid-phase reactions, high proportions of nitrogen-containing or sulfur-containing compounds are typically considered anthropogenic primary emissions or classes of relatively stable compounds in SOA that related terminal oxidation for oxygenated OA under high-NO_x conditions (Han et al., 2023; Fan et al., 2022; Jiang et al., 2023). In fact, as the NO_x concentration during the entire sampling period was less than 10% of O_3 , our results may indicate that the oxidation processes cannot effectively transform the oxygenated OA into nitrogen-containing or sulfur-containing compounds.

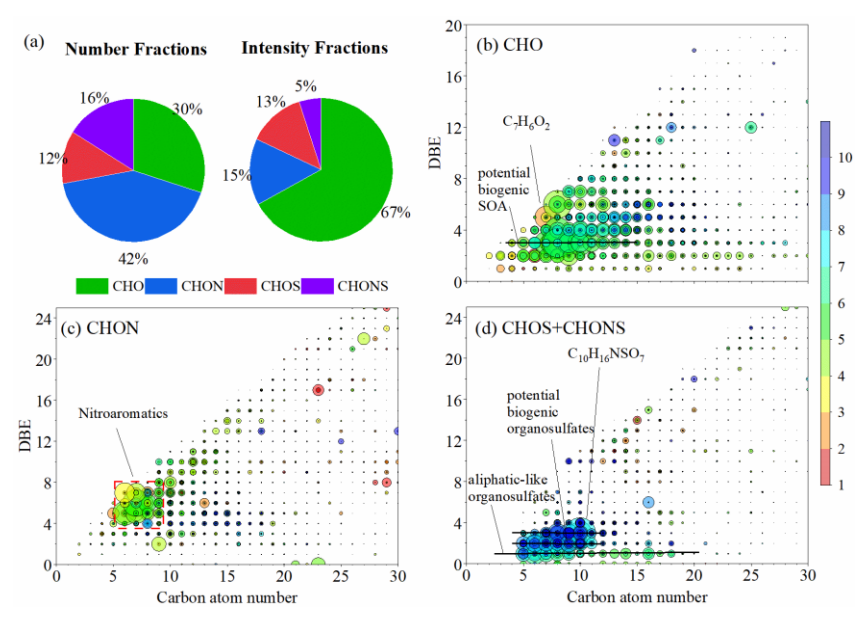


Figure 3: Molecular characteristics of OA. (a) Average proportions of elemental compound groups, presented by both formula count and intensity. (b-d) Double bond equivalent (DBE) vs. Carbon number plots for CHO, CHON, and organosulfur compounds (CHOS+CHONS). Marker size denotes the average peak intensities of the compounds, while the colour bar represents the oxygen number, O/N, and O/S ratios using a consistent gradient.

Previous studies have indicated that ESI- is more inclined to detect oxidized and polar compounds (Lin et al., 2012; Jiang et al., 2016). Figures 3b-d and Figure S10 show the molecular distribution of compound groups detected in this study. Among the detected CHO compounds, C8-12 species are the most abundant, accounting for over 50% of the total intensity. Several high-intensity compounds, such as C₈H₁₂O₄₋₆, C₈H₁₀O₅, C₉H₁₄O₅₋₆, and C₁₀H₁₆O₅ have been commonly detected in laboratory simulation studies and environmental samples and are considered monoterpene-SOA components (Table S3) (Romonosky et al., 2015; Xu et al., 2021). However, compounds with the same molecular formulas have also been identified in biomass burning aerosols (Wang et al., 2017c) and SOA derived from aromatic oxidation (Mehra et al., 2020; Kumar et al., 2023). In this study, positive correlations were observed not only between these compounds and biogenic species (Figure S11) but also with anthropogenic VOCs and SOA tracers, indicating their multiple sources—_Even if these compounds were derived from the oxidation of biogenic VOCs, the influence of anthropogenic emissions could not be ruled out, as biomass burning and cooking are also important sources of –biogenic VOCs (Zhang et al., 2025; Song et al., 2022). The intensities of these

compounds were positively correlated with typical tracers for cooking and its atmospheric oxidation products (*i.e.*, oleic and azelaic acids) (Xu et al., 2023; Bikkina et al., 2014), but not with levoglucosan, supporting the potential origins from cooking for these compounds. Due to the lack of corresponding structural information, it is challenging to determine the specific sources of these compounds.

It is important to note that the oxidation of aromatic VOCs is an important source of OA in this study. A series of anthropogenic-related compounds were detected in our samples, exhibiting high abundance, such as $C_7H_6O_2$, $C_8H_6O_4$, and $C_7H_{10}O_5$. Additionally, abundant CHON compounds were detected, with C_6 - C_{10} nitroaromatic compounds dominating the total intensity. Nitroaromatic compounds are widely observed in environmental aerosols and are primarily derived from the oxidation of anthropogenic-related VOCs, particularly those associated with biomass burning OAs (Xie et al., 2017; Li et al., 2019; Cai et al., 2022). Overall, molecular-level analysis based on offline HR-MS data indicated that secondary SOA formation from both anthropogenic and biogenic emissions was the main source of OA during the study period. This highlights the complex interplay between different emission sources and the transformation processes contributing to OA composition.

335 3.4 Molecular associations with sources and SOA processes

340

355

Although previous source apportionment methods using molecular composition data from various online mass spectrometers (e.g., EESI-TOF-MS) have been widely applied to determine the source of OA (Ge et al., 2024), these methods have primarily focused on specific fractions of OA, such as CHO and CHON compounds, due to their importance as precursors of particle SOA (Zheng et al., 2023; Ge et al., 2024). To further understand the impact of PMF-resolved sources and SOA processes on OA formation at the molecular level, a constrained-NMF model was applied by simultaneously incorporating the six PMF factors and the molecules identified by HR-MS analysis. It is noteworthy that while the hourly concentrations of each PMF factor are independent, significant correlations were found between the daily-average concentrations of MT-SOA, Iso-SOA, and eookingC-OA, aligning with the time windows of PM25 samples. As a result, an independent MT-SOA factor could not be obtained in our constrained-NMF model (Figure 4), as it was mainly shared by the NMF factors of Iso-SOA and C-OAcooking (referred as Iso-SOA_{NMF} and C-OA_{NMF}, same for other factors). However, the model effectively distinguished the BB-OA, gas-pSOA, and SIA-OA factors resolved by tracer-based PMF model. Overall, the five-factor solution explained over 99% of the total variance, allowing for the identification of molecules associated with each tracerbased PMF factor. It should be noted that the mass spectra of all factors resolved by the eonstrained-NMF model might differ from those of source samples or laboratory-generated SOA, as our results primarily reflected the characteristics of each tracer-based PMF factor observed in the real ambient atmosphere (Mo et al., 2024). The compounds identified in each NMF factor may not fully correspond to the names of the PMF factors, as PMF factors represent not only specific sources but also indicate that certain compounds may share similar formation pathways with the atmospheric processes implied by the factor names. For example, in the Iso-SOA_{NMF} factor, many anthropogenic-related compounds might also be present alongside biogenic SOA, suggesting that these anthropogenic compounds could have similar atmospheric formation pathways as biogenic SOA.

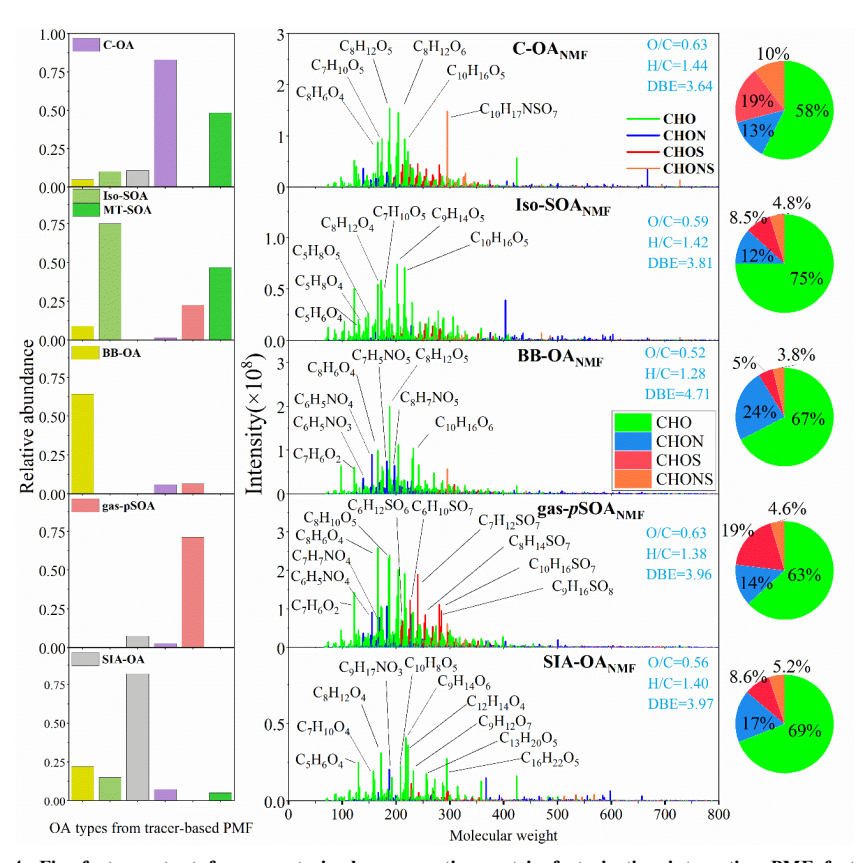


Figure 4: Five-factor output from constrained non-negative matrix factorization integrating PMF factors and molecular composition data. On the left, the chart displays the percentages of PMF factors contributing to each NMF factor. In the center, the factor spectra are shown, with several intense species highlighted. On the right, the percentages of different compound groups are presented.

Figure 4 presents the mass spectra for each factor obtained from the constrained-NMF analysis, with several highly intense species also indicated. As shown in Table S4, which summarizes the average chemical parameters of each NMF factor, the C-OA_{NMF} was featured by the highest O/C ratio and the lowest DBE value. Within this factor, a series of highly abundant compounds, including C₈H₁₂O₅, C₈H₁₀O₅, C₈H₁₂O₄, C₉H₁₄O₅, C₈H₁₂O₆, C₁₀H₁₆O₅ and C₉H₁₄O₆, were observed. As previously

mentioned, these compounds may originate from the oxidation of monoterpenes emitted from both biological sources and cooking. Previous studies have suggested that although alkanals, alkenals, and alkadienals are identified as the main types of emissions from cooking, their proportion in household cooking emissions in China is relatively small. This indicates that the precursors and SOA formed from cooking oil heating emissions may not fully represent the precursors and SOA formed from real-world cooking emissions (Yu et al., 2022; Song et al., 2022). A recent study has shown that even during the cooking process of fried foods, emissions of oleic acid and linoleic acid are relatively low compared to aromatic hydrocarbons (Song et al., 2022; Song et al., 2023). Therefore, the presence of some high-abundance aromatic compounds, such as C₇H₆O₂, in this factor is reasonable. Additionally, oxygen-containing compounds, especially short-chain acids and aldehydes (*i.e.*, hexanoic acid, hexanal, and nonanal), are abundant in cooking vapor. These short-chain acids can react with SO₂ in the atmosphere to form organosulfates (Passananti et al., 2016; Zhu et al., 2019), which explains the high abundance of C6 organosulfate compounds observed in the C-OA_{NMF} factor. Notably, we also observed a high abundance of C₁₀H₁₇NSO₇, a typical nitrooxy organosulfate generated by the atmospheric oxidation of monoterpenes (Surratt et al., 2008).

The Iso-SOA_{NMF} exhibited an O/C ratio similar to that of C-OA_{NMF} but had the highest effective oxidation number (nO_{eff}) values among all NMF factors (Table S4). This observation supports our earlier speculation that the elevated oxidation level of MO-OOA in AMS-PMF derived OA components could be attributed to significant contributions from Iso-SOA. In addition to several highly intense monoterpene SOA species, a series of C_5 oxygen-containing compounds, such as $C_5H_{6-8}O_4$ and $C_5H_{6-8}O_5$, also displayed high intensity in the Iso-SOA_{NMF} factor (Figure 4). However, due to the lower ionization efficiency of ESI-for compounds with fewer than six carbon atoms (Kebarle and Tang, 1993), the abundance of these C_5 compounds is not as high as that of C_{6-8} compounds.

The BB-OA_{NMF} factor showed the lowest O/C and H/C ratios but the highest DBE and AI values compared to other NMF factors (Table S4), indicating its high aromaticity. This factor contained not only monoterpene SOA but was also rich in oxygen-containing aromatic compounds (e.g., C₇H₆O₂₋₃, C₈H₈O₃, and C₈H₆O₄₋₅). These compounds are potential phenolic substances that may originate from the pyrolysis of lignin (Siemens et al., 2023; Kawamoto, 2017; Lin et al., 2016). Importantly, the mass spectrum of this factor included a large fraction of nitrogen-containing compounds, particularly nitrophenols (e.g., C₆H₅NO₃, C₆H₅NO₄, C₇H₅NO₅, and C₈H₇NO₅). Nitrophenols have been widely reported in both fresh and aged biomass burning OAs, primarily formed by the reaction of phenolic compounds from lignin pyrolysis with inorganic nitrogen (Li et al., 2019; Lin et al., 2017; Song et al., 2018).

The gas-pSOA_{NMF} factor contained a high abundance of aromatic-CHO compounds, nitroaromatic compounds, and CHOS compounds (Figure 4). The chemical processes involved in gas-phase reactions are relatively complex. On one hand, the high abundance of C8-C10 aromatic-CHO compounds may result from the photo-oxidation of PAHs (Keyte et al., 2013), and some nitroaromatic compounds can also be generated through gas-phase photochemical reactions (Cai et al., 2022; Fan et al., 2022). Given the high RH during the sampling period, the uptake of SO₂ by VOCs in the gas phase is a primary pathway for the generation of organosulfates (Bruggemann et al., 2020; Ye et al., 2018). Although the atmospheric SIA formation processes are also complex and may partially overlap with gas-pSOA processes, gas-phase oxidation (both daytime •OH

oxidation and nighttime NO₃• oxidation) remains a major formation pathway for SIA (Zhu et al., 2023). Our results indicated that sulfur additions were less significant compared to gas-pSOA processes. As mentioned earlier, we found that variations in SIA-OA were potentially affected by the nocturnal oxidation of VOCs (NO₃•/O₃ oxidation). Notably, nighttime organic nitrates generally formed through reactions between NO₃• and alkenes in the gas phase, with NO₃• adding to the double bond of unsaturated VOCs to generate alkene-like organic nitrates (Ng et al., 2017; Fan et al., 2022). A higher proportion of alkene-like CHON compounds was observed in the SIA-OA_{NMF} (21%) compared to the gas-pSOA_{NMF} factor (8%), with the compound C₉H₁₇NO₃ (DBE=2) showing the highest average intensity in SIA-OA_{NMF}. These findings collectively support the influence of nocturnal oxidation on the formation of SIA-OA.

400

405

410

420

Figure 5 illustrates the relative abundance of molecules identified by the PMF factor-constrained NMF method as a proportion of the total identified compounds. Notably, the contributions of biogenic SOA, cooking and BB to OA derived from the molecular composition-based NMF analysis aligned with the results from the tracer-based PMF model. However, the contribution of gas-pSOA to OA from the NMF method was 1.4 times that of the PMF model, while the contribution of SIA-OA to OA was only 1/3 of the PMF model's estimate. Although the tracer-based PMF model can mathematically separate atmospheric SOA processes into SIA and gas-pSOA, these categories may still partially overlap in real-world conditions. As discussed above, gas-phase oxidation, particularly nocturnal oxidation, is a major pathway for SIA formation. Our results suggest that, in the NMF analysis, many compounds associated with SIA processes may have been over-attributed to gaspSOA, potentially leading to an underestimation of the contribution of nocturnal oxidation to SOA formation. However, given the relatively stable levels of SIA-OA observed during the sampling period, and considering that misclassification between SIA-related and gas-pSOA-related species did not affect the contributions from other sources (BB, biogenic SOA, and cooking) or the total SOA contributions, the results from the molecule-based NMF analysis remain reasonably robust. Importantly, both methods consistently indicated that gas-phase oxidation of VOCs was a significant pathway for OA formation throughout the study period, particularly for anthropogenic VOCs. This is evidenced by the relative abundance of potential aromatic compounds (DBE≥4), which ranged from 45% to 61% in the NMF factors, highlighting the substantial impact of anthropogenic emissions on OA formation in this study.

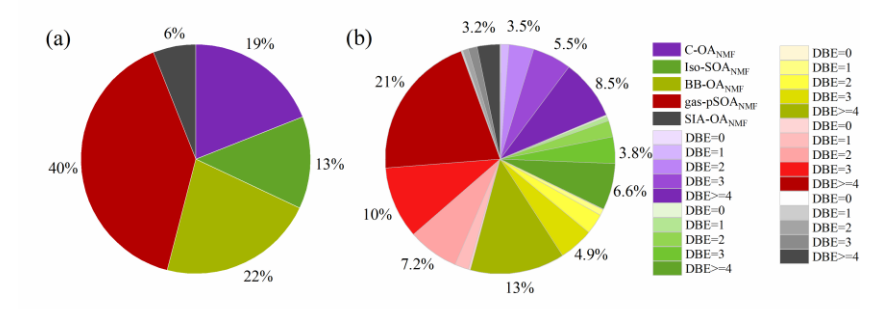


Figure 5: (a) Intensity-based source contributions of each NMF-factor and (b) corresponding classifications based on DBE values. Compounds with DBE values greater than 4 are tentatively considered to possess benzene structures or originate from anthropogenic sources. Relative intensities below 3% are not labelled.

4 Conclusions

435

440

This study offers a comprehensive understanding of the sources and formation pathways of OA at a background site in Hong Kong by integrating OA composition data from online AMS, SOA tracers from TAG-TOF-MS analysis, and molecular composition from offline HR-MS. Our findings indicate that biomass burning and gas-pSOA were the main sources of low-oxidationLO-O OA during the COVID-19 lockdown, influenced by air mass transport from mainland China. In contrast, SIA-OA, gas-pSOA and biogenic SOA accounted for over 90% of high-oxidation MO-OOA, with Iso-SOA being a dominant contributor to the high oxidation level-of OA. HR-MS analysis revealed that CHO and CHON compounds were significant components of OA, contributing over 60% of the total intensity and over 40% of the formula count, respectively. This suggests that atmospheric oxidation processes significantly led to the accumulation of a few CHO compounds, while nitrogen-addition reactions increased the diversity of the molecular composition.

Given the complexity of atmospheric chemical processes and the diverse sources of OA substances, relying solely on non-targeted molecular composition for PMF analysis can pose challenges in factor interpretation. The molecular composition-based NMF model, constrained by PMF factors, enhances the interpretability of these factors and further elucidates the intrinsic molecular composition differences among sources and formation pathways. For instance, our analysis revealed that gas-pSOA is more conducive to forming S-containing organic compounds, whereas the SIA process tends to produce more nonaromatic CHON compounds. Ultimately, the source apportionment results from the NMF analysis showed strong consistency with those from the PMF analysis, both underscoring the significant impact of anthropogenic emissions on OA formation during the sampling period.

Hong Kong, a highly developed city with a dense population, has maintained relatively low PM_{2.5} concentrations compared to mainland China. However, further reducing PM_{2.5} levels to meet WHO standards remains a big challenge. Our findings indicate that regional transport of anthropogenic emissions from mainland China continues to be a major factor influencing OA formation in Hong Kong. During autumn days with frequent photochemical reactions, the combination of anthropogenic pollutants and local biogenic VOCs contributes to SOA generation. Therefore, effectively reducing PM_{2.5} pollution in Hong Kong requires not only local emission reductions but also regional cooperation. Given China's substantial progress in mitigating PM_{2.5} pollution and the anticipated further decreases in atmospheric PM_{2.5} concentrations with the implementation of policies such as the Double-Carbon Policy, this research offers valuable insights into the sources and formation of OA under low PM pollution conditions. These insights are crucial for developing effective particulate matterPM_{2.5} control measures in the future.

设置了格式:下标设置了格式:下标

455 Data availability

The authors comply with ACP's open data policy, and the data supporting this paper was uploaded on Zenodo (Jiang et al., 2025) and can be available at https://zenodo.org/records/15675889, which includes the original data for the AMS and HPLC-HR-MS analysis, and the detailed data for figures appeared in the main text.

Author contributions

460 H.J., F.W., Y.C. and H.G. designed the study, Y.H. conducted the field measurements, Y.D. and Y.H. helped the online data analysis, H.J and Y.C. performed the HPLC-HRMS analysis and data processing. H. G. acquired funding and undertook project management; H.J. prepared the manuscript with contributions from all coauthors.

Competing interests

The authors declare that they have no conflict of interest.

465 Acknowledgements

This project is supported by the Research Grants Council of the Hong Kong Special Administrative Region via General Research Fund scheme (PolyU 152124/21E), Theme-based Research Scheme (T24-508/22-N), the Research Institute for Land and Space of the Hong Kong Polytechnic University via RILS Strategic Support Scheme (SSS) Fund (1-CDLJ) and Matching Fund Scheme (1-CDM6), and the National Natural Science Foundation of China (grant nos. 42407144).

470 References

- An, Z., Huang, R. J., Zhang, R., Tie, X., Li, G., Cao, J., Zhou, W., Shi, Z., Han, Y., Gu, Z., and Ji, Y.: Severe haze in northern China: A synergy of anthropogenic emissions and atmospheric processes, Proceedings of the National Academy of Sciences of the United States of America, 116, 8657-8666, doi:10.1073/pnas.1900125116, 2019.
- Bikkina, S., Kawamura, K., Miyazaki, Y., and Fu, P.: High abundances of oxalic, azelaic, and glyoxylic acids and methylglyoxal in the open ocean with high biological activity: Implication for secondary OA formation from isoprene, Geophysical Research Letters, 41, 3649-3657, doi:10.1002/2014gl059913, 2014.
 - Bruggemann, M., Xu, R., Tilgner, A., Kwong, K. C., Mutzel, A., Poon, H. Y., Otto, T., Schaefer, T., Poulain, L., Chan, M. N., and Herrmann, H.: Organosulfates in Ambient Aerosol: State of Knowledge and Future Research Directions on Formation, Abundance, Fate, and Importance, Environmental Science & Technology, 54, 3767-3782, doi:10.1021/acs.est.9b06751, 2020.
- Cai, D., Wang, X., George, C., Cheng, T., Herrmann, H., Li, X., and Chen, J.: Formation of Secondary Nitroaromatic Compounds in Polluted Urban Environments, Journal of Geophysical Research: Atmospheres, 127, e2021JD036167, doi:10.1029/2021jd036167, 2022.
 Daellenbach, K. R., Uzu, G., Jiang, J., Cassagnes, L. E., Leni, Z., Vlachou, A., Stefenelli, G., Canonaco, F., Weber, S., Segers, A., Kuenen, J. J. P., Schaap, M., Favez, O., Albinet, A., Aksoyoglu, S., Dommen, J., Baltensperger, U., Geiser, M., El Haddad, I., Jaffrezo, J. L., and Prevot, A. S. H.: Sources of particulate-matter air pollution and its oxidative potential in Europe, Nature, 587, 414-419, doi:10.1038/s41586-485
 - Ding, X., Wang, X.-M., and Zheng, M.: The influence of temperature and aerosol acidity on biogenic secondary organic aerosol tracers: Observations at a rural site in the central Pearl River Delta region,
 South China, Atmospheric Environment, 45, 1303-1311, doi:10.1016/j.atmosenv.2010.11.057, 2011.

- Ding, X., Zhang, Y.-Q., He, Q.-F., Yu, Q.-Q., Shen, R.-Q., Zhang, Y., Zhang, Z., Lyu, S.-J., Hu, Q.-H., Wang, Y.-S., Li, L.-F., Song, W., and Wang, X.-M.: Spatial and seasonal variations of secondary organic aerosol from terpenoids over China, Journal of Geophysical Research: Atmospheres, 121, 14,661-614,678, doi:10.1002/2016jd025467, 2016.

 Ditto, J. C., Barnes, E. B., Khare, P., Takeuchi, M., Joo, T., Bui, A. A. T., Lee-Taylor, J., Eris, G., Chen, Y., Aumont, B., Jimenez, J. L., Ng, N. L., Griffin, R. J., and Gentner, D. R.: An omnipresent diversity and variability in the chemical composition of atmospheric functionalized
- organic aerosol, Communications Chemistry, 1, 75, doi:10.1038/s42004-018-0074-3, 2018.

 Ervens, B., Rickard, A., Aumont, B., Carter, W. P. L., McGillen, M., Mellouki, A., Orlando, J., Picquet-Varrault, B., Seakins, P., Stockwell, W. R., Vereecken, L., and Wallington, T. J.: Opinion: Challenges and needs of tropospheric chemical mechanism development, Atmospheric
- Chemistry and Physics, 24, 13317-13339, doi:10.5194/acp-24-13317-2024, 2024.

 Fan, W., Chen, T., Zhu, Z., Zhang, H., Qiu, Y., and Yin, D.: A review of secondary organic aerosols formation focusing on organosulfates and organic nitrates, Journal of Hazardous Materials, 430, 128406, doi:10.1016/j.jhazmat.2022.128406, 2022.
- 500 Fu, P., Kawamura, K., and Miura, K.: Molecular characterization of marine organic aerosols collected during a round-the-world cruise, Journal of Geophysical Research, 116, D13302, doi:10.1029/2011JD015604, 2011.
 Gao, Y., Lee, S.-C., Huang, Y., Chow, J. C., and Watson, J. G.: Chemical characterization and source apportionment of size-resolved particles in Hong Kong sub-urban area, Atmospheric Research, 170, 112-122, doi:10.1016/j.atmosres.2015.11.015, 2016.
 Ge, D., Nie, W., Liu, Y., Huang, D. D., Yan, C., Wang, J., Li, Y., Liu, C., Wang, L., Wang, J., Chi, X., and Ding, A.: New Insights Into the
- 505 Sources of Atmospheric Organic Aerosols in East China: A Comparison of Online Molecule-Level and Bulk Measurements, Journal of Geophysical Research: Atmospheres, 129, e2024JD040768, doi:10.1029/2024jd040768, 2024.
 Geng, X., Zhong, G., Li, J., Cheng, Z., Mo, Y., Mao, S., Su, T., Jiang, H., Ni, K., and Zhang, G.: Molecular marker study of aerosols in the northern South China Sea: Impact of atmospheric outflow from the Indo-China Peninsula and South China, Atmospheric Environment, 206, 225-236, doi:10.1016/j.atmosenv.2019.02.033, 2019.
- 510 Han, Y., Zhang, X., Li, L., Lin, Y., Zhu, C., Zhang, N., Wang, Q., and Cao, J.: Enhanced Production of Organosulfur Species during a Severe Winter Haze Episode in the Guanzhong Basin of Northwest China, Environmental Science & Technology, 57, 8708-8718, doi:10.1021/acs.est.3c02914, 2023.
 Hopke, P. K.: Review of receptor modeling methods for source apportionment, Journal of The Air & Waste Management Association, 66.
- 237-259, doi:10.1080/10962247.2016.1140693, 2016.
 515 Hoyle, C. R., Berntsen, T., Myhre, G., and Isaksen, I. S. A.: Secondary organic aerosol in the global aerosol chemical transport model Oslo CTM2, Atmospheric Chemistry and Physics, 7, 5675-5694, doi:10.5194/acp-7-5675-2007, 2007.
 - Huang, D. D., Zhu, S., An, J., Wang, Q., Qiao, L., Zhou, M., He, X., Ma, Y., Sun, Y., Huang, C., Yu, J. Z., and Zhang, Q.: Comparative Assessment of Cooking Emission Contributions to Urban Organic Aerosol Using Online Molecular Tracers and Aerosol Mass Spectrometry Measurements, Environmental Science & Technology, 55, 14526-14535, doi:10.1021/acs.est.1c03280, 2021.
- 520 Huo, Y., Yao, D., and Guo, H.: Differences in aerosol chemistry at a regional background site in Hong Kong before and during the COVID-19 pandemic, Science of the Total Environment, 926, 171990, doi:10.1016/j.scitotenv.2024.171990, 2024a.
 Huo, Y., Lyu, X., Yao, D., Zhou, B., Yuan, Q., Lee, S. c., and Guo, H.: Exploring the Formation of High Levels of Hydroxyl Dicarboxylic Acids at an Urban Background Site in South China, Journal of Geophysical Research: Atmospheres, 129, e2023JD040096, doi:10.1029/2023jd040096, 2024b.
- 525 Jiang, B., Kuang, B. Y., Liang, Y., Zhang, J., Huang, X. H. H., Xu, C., Yu, J. Z., and Shi, Q.: Molecular composition of urban organic aerosols on clear and hazy days in Beijing: a comparative study using FT-ICR MS, Environmental Chemistry, 13, 888-901, doi:10.1071/en15230, 2016.
- Jiang, H., Cai, J., Feng, X., Chen, Y., Li, J., and Zhang, G.: Sources and composition of elemental carbon during haze events in North China by a high time-resolved study, Science of The Total Environment, 907, 168055, doi:10.1016/j.scitotenv.2023.168055, 2024.
 Jiang, H., Deng, Y., Huo, Y., Wang, F., Chen, Y., and Guo, H.: Molecular Insights into Organic Aerosol Sources and Formation at a Regional
- Background Site in South China [Data set], Zenodo, https://doi.org/10.5281/zenodo.15675889, 2025.

 Jiang, H., Cai, J., Feng, X., Chen, Y., Wang, L., Jiang, B., Liao, Y., Li, J., Zhang, G., Mu, Y., and Chen, J.: Aqueous-Phase Reactions of Anthropogenic Emissions Lead to the High Chemodiversity of Atmospheric Nitrogen-Containing Compounds during the Haze Event, Environmental Science & Technology, 57, 16500-16511, doi:10.1021/acs.est.3c06648, 2023.
- 535 Jimenez, J. L., Canagaratna, M. R., Donahue, N. M., Prevot, A. S. H., Zhang, Q., Kroll, J. H., DeCarlo, P. F., Allan, J. D., Coe, H., Ng, N. L., Aiken, A. C., Docherty, K. S., Ulbrich, I. M., Grieshop, A. P., Robinson, A. L., Duplissy, J., Smith, J. D., Wilson, K. R., Lanz, V. A., Hueglin, C., Sun, Y. L., Tian, J., Laaksonen, A., Raatikainen, T., Rautiainen, J., Vaattovaara, P., Ehn, M., Kulmala, M., Tomlinson, J. M., Collins, D. R., Cubison, M. J., Dunlea, J., Huffman, J. A., Onasch, T. B., Alfarra, M. R., Williams, P. I., Bower, K., Kondo, Y., Schneider, J., Drewnick, F., Borrmann, S., Weimer, S., Demerjian, K., Salcedo, D., Cottrell, L., Griffin, R., Takami, A., Miyoshi, T., Hatakeyama, S.,
- 540 Shimono, A., Sun, J. Y., Zhang, Y. M., Dzepina, K., Kimmel, J. R., Sueper, D., Jayne, J. T., Herndon, S. C., Trimborn, A. M., Williams, L. R., Wood, E. C., Middlebrook, A. M., Kolb, C. E., Baltensperger, U., and Worsnop, D. R.: Evolution of Organic Aerosols in the Atmosphere, Science, 326, 1525, doi:10.1126/science.1180353, 2009.
 Kanakidou, M. Scinfeld, J. H. Pandie, S. N. Barnes, L. Dentener, F. L. Facchini, M. C. Dingener, R. V. Ervens, R. Nenes, A. Nielsen, A. Niel
 - Kanakidou, M., Seinfeld, J. H., Pandis, S. N., Barnes, I., Dentener, F. J., Facchini, M. C., Dingenen, R. V., Ervens, B., Nenes, A., Nielsen, C. J., Swietlicki, E., Putaud, J. P., Balkanski, Y., Fuzzi, S., Horth, J., Moortgat, G. K., R. Winterhalter, Myhre, C. E. L., Tsigaridis, K., Vignati,

- 545 E., Stephanou, E. G., and, and J.Wilson: Organic aerosol and global climate modelling: a review, Atmospheric Chemistry and Physics, 5, 1053–1123, doi:10.5194/acp-5-1053-2005, 2005, 2005.
 Kawamoto, H.: Lignin pyrolysis reactions, Journal of Wood Science, 63, 117-132, doi:10.1007/s10086-016-1606-z, 2017.
 - Kebarle, P. and Tang, L.: From ions in solution to ions in the gas phase the mechanism of electrospray mass spectrometry, Analytical Chemistry, 65, 972A-986A, doi:10.1021/ac00070a001, 1993.
- Keyte, I. J., Harrison, R. M., and Lammel, G.: Chemical reactivity and long-range transport potential of polycyclic aromatic hydrocarbons-a review, Chemical Society Reviews, 42, 9333-9391, doi:10.1039/c3cs60147a, 2013.
 Kumar, V., Slowik, J. G., Baltensperger, U., Prevot, A. S. H., and Bell, D. M.: Time-Resolved Molecular Characterization of Secondary Organic Aerosol Formed from OH and NO3 Radical Initiated Oxidation of a Mixture of Aromatic Precursors, Environmental Science & Technology, 57, 11572-11582, doi:10.1021/acs.est.3c00225, 2023.
- Laskin, J., Laskin, A., and Nizkorodov, S. A.: Mass Spectrometry Analysis in Atmospheric Chemistry, Analytical Chemistry, 90, 166-189, doi:10.1021/acs.analchem.7b04249, 2018.
 Li, C., He, Q., Hettiyadura, A. P., S., Kafer, U., Shmul, G., Meidan, D., Zimmermann, R., Brown, S. S., George, C., Laskin, A., and Rudich, Y.: Formation of Secondary Brown Carbon in Biomass Burning Aerosol Proxies through NO3 Radical Reactions, Environmental Science & Technology, 54, 1395–1405, doi:10.1021/acs.est.9b05641, 2019.
- 560 Li, H., Duan, F., Ma, T., Ma, Y., Xu, Y., Wang, S., Zhang, Q., Jiang, J., Zhu, L., Li, F., Huang, T., Kimoto, T., and He, K.: Molecular Characterization of Organosulfur and Organonitrogen Compounds in Summer and Winter PM(2.5) via UHPLC-Q-Orbitrap MS/MS, Environmental Science & Technology, 58, 21692–21701, doi:10.1021/acs.est.4c02727, 2024.
 Li, J. J., Wang, G. H., Cao, J. J., Wang, X. M., and Zhang, R. J.: Observation of biogenic secondary organic aerosols in the atmosphere of a mountain site in central China: temperature and relative humidity effects, Atmospheric Chemistry and Physics, 13, 11535-11549,
- 565 doi:10.5194/acp-13-11535-2013, 2013a. Li, Y. J., Lee, B. Y. L., Yu, J. Z., Ng, N. L., and Chan, C. K.: Evaluating the degree of oxygenation of organic aerosol during foggy and hazy days in Hong Kong using high-resolution time-of-flight aerosol mass spectrometry (HR-ToF-AMS), Atmospheric Chemistry and Physics, 13, 8739-8753, doi:10.5194/acp-13-8739-2013, 2013b.
- Lin, P., Rincon, A. G., Kalberer, M., and Yu, J. Z.: Elemental Composition of HULIS in the Pearl River Delta Region, China: Results
 Inferred from Positive and Negative Electrospray High Resolution Mass Spectrometric Data, Environmental Science & Technology, 46, 7454-7462, doi:10.1021/es300285d, 2012.
 Lin, P., Bluvshtein, N., Rudich, Y., Nizkorodov, S. A., Laskin, J., and Laskin, A.: Molecular Chemistry of Atmospheric Brown Carbon Inferred from a Nationwide Biomass Burning Event, Environmental Science & Technology, 51, 11561-11570, doi:10.1021/acs.est.7b02276, 2017
- 575 Lin, P., Aiona, P. K., Li, Y., Shiraiwa, M., Laskin, J., Nizkorodov, S. A., and Laskin, A.: Molecular Characterization of Brown Carbon in Biomass Burning Aerosol Particles, Environmental Science & Technology, 50, 11815-11824, doi:10.1021/acs.est.6b03024, 2016.
 Liu, L., Hohaus, T., Franke, P., Lange, A. C., Tillmann, R., Fuchs, H., Tan, Z., Rohner, F., Karydis, V., He, Q., Vardhan, V., Andres, S., Bohn, B., Holland, F., Winter, B., Wedel, S., Novelli, A., Hofzumahaus, A., Wahner, A., and Kiendler-Scharr, A.: Observational evidence reveals the significance of nocturnal chemistry in seasonal secondary organic aerosol formation, npj Climate and Atmospheric Science, 7,
 - 207, doi:10.1038/s41612-024-00747-6, 2024.

 Lopez-Hilfiker, F. D., Pospisilova, V., Huang, W., Kalberer, M., Mohr, C., Stefenelli, G., Thornton, J. A., Baltensperger, U., Prevot, A. S. H., and Slowik, J. G.: An extractive electrospray ionization time-of-flight mass spectrometer (EESI-TOF) for online measurement of atmospheric aerosol particles, Atmospheric Measurement Techniques, 12, 4867-4886, doi:10.5194/amt-12-4867-2019, 2019.

 Lyu, X., Li, H., Lee, S. C., Xiong, E., Guo, H., Wang, T., and de Gouw, J.: Significant Biogenic Source of Oxygenated Volatile Organic
- 585 Compounds and the Impacts on Photochemistry at a Regional Background Site in South China, Environmental Science & Technology, 58, 20081–20090, doi:10.1021/acs.est.4c05656, 2024.
 Lyu, X., Guo, H., Yao, D., Lu, H., Huo, Y., Xu, W., Kreisberg, N., Goldstein, A. H., Jayne, J., Worsnop, D., Tan, Y., Lee, S. C., and Wang, T.: In Situ Measurements of Molecular Markers Facilitate Understanding of Dynamic Sources of Atmospheric Organic Aerosols, Environmental Science & Technology, 54, 11058-11069, doi:10.1021/acs.est.0c02277, 2020.
- Mahowald, N.: Aerosol Indirect Effect on Biogeochemical Cycles and Climate, Science, 334, 794-796, doi:10.1126/science.1207374, 2011.
 Mehra, A., Wang, Y., Krechmer, J. E., Lambe, A., Majluf, F., Morris, M. A., Priestley, M., Bannan, T. J., Bryant, D. J., Pereira, K. L., Hamilton, J. F., Rickard, A. R., Newland, M. J., Stark, H., Croteau, P., Jayne, J. T., Worsnop, D. R., Canagaratna, M. R., Wang, L., and Coe, H.: Evaluation of the chemical composition of gas- and particle-phase products of aromatic oxidation, Atmospheric Chemistry and Physics, 20, 9783-9803, doi:10.5194/acp-20-9783-2020, 2020.
- 595 Mo, Y., Li, J., Zhong, G., Zhu, S., Cheng, Z., Tang, J., Jiang, H., Jiang, B., Liao, Y., Song, J., Tian, C., Chen, Y., Zhao, S., and Zhang, G.: The Sources and Atmospheric Processes of Strong Light-Absorbing Components in Water Soluble Brown Carbon: Insights From a Multi-Proxy Study of PM2.5 in 10 Chinese Cities, Journal of Geophysical Research: Atmospheres, 129, e2023JD039512, doi:10.1029/2023jd039512, 2024.
- Monti, S., Tamayo, P., Mesirov, J., and Golub, T.: Consensus Clustering: A Resampling-Based Method for Class Discovery and Visualization of Gene Expression Microarray Data, Machine Learning, 52, 91-118, doi:10.1023/A:1023949509487, 2003.

- Ng, N. L., Brown, S. S., Archibald, A. T., Atlas, E., Cohen, R. C., Crowley, J. N., Day, D. A., Donahue, N. M., Fry, J. L., Fuchs, H., Griffin, R. J., Guzman, M. I., Herrmann, H., Hodzic, A., Iinuma, Y., Jimenez, J. L., Kiendler-Scharr, A., Lee, B. H., Luecken, D. J., Mao, J., McLaren, R., Mutzel, A., Osthoff, H. D., Ouyang, B., Picquet-Varrault, B., Platt, U., Pye, H. O. T., Rudich, Y., Schwantes, R. H., Shiraiwa, M., Stutz, J., Thornton, J. A., Tilgner, A., Williams, B. J., and Zaveri, R. A.: Nitrate radicals and biogenic volatile organic compounds: oxidation,
- mechanisms, and organic aerosol, Atmospheric Chemistry and Physics, 17, 2103-2162, doi:10.5194/acp-17-2103-2017, 2017.
 Nie, W., Yan, C., Huang, D. D., Wang, Z., Liu, Y., Qiao, X., Guo, Y., Tian, L., Zheng, P., Xu, Z., Li, Y., Xu, Z., Qi, X., Sun, P., Wang, J., Zheng, F., Li, X., Yin, R., Dallenbach, K. R., Bianchi, F., Petäjä, T., Zhang, Y., Wang, M., Schervish, M., Wang, S., Qiao, L., Wang, Q., Zhou, M., Wang, H., Yu, C., Yao, D., Guo, H., Ye, P., Lee, S., Li, Y. J., Liu, Y., Chi, X., Kerminen, V.-M., Ehn, M., Donahue, N. M., Wang, T., Huang, C., Kulmala, M., Worsnop, D., Jiang, J., and Ding, A.: Secondary organic aerosol formed by condensing anthropogenic vapours over China's megacities, Nature Geoscience, 15, 255-261, doi:10.1038/s41561-022-00922-5, 2022.
- Norris, G., Duvall, R., Brown, S., and Bai, S.: EPA Positive Matrix Factorization (PMF) 5.0 Fundamentals and User Guide Prepared for the US Environmental Protection Agency Office of Research and Development, 2014.

 Noziere, B., Kalberer, M., Claevs, M., Allan, J., D'Anna, B., Decesari, S., Finessi, E., Glasius, M., Grgic, I., Hamilton, J. F., Hoffmann, T.,

linuma, Y., Jaoui, M., Kahnt, A., Kampf, C. J., Kourtchev, I., Maenhaut, W., Marsden, N., Saarikoski, S., Schnelle-Kreis, J., Surratt, J. D.,

- 615 Szidat, S., Szmigielski, R., and Wisthaler, A.: The molecular identification of organic compounds in the atmosphere: state of the art and challenges, Chemical Reviews, 115, 3919-3983, doi:10.1021/cr5003485, 2015.
 Passananti, M., Kong, L., Shang, J., Dupart, Y., Perrier, S., Chen, J., Donaldson, D. J., and George, C.: Organosulfate Formation through the Heterogeneous Reaction of Sulfur Dioxide with Unsaturated Fatty Acids and Long-Chain Alkenes, Angewandte Chemie International Edition, 55, 10336-10339, doi:10.1002/anie.201605266, 2016.
- 620 Pye, H. O. T., Chan, A. W. H., Barkley, M. P., and Seinfeld, J. H.: Global modeling of organic aerosol: the importance of reactive nitrogen (NOx and NO3), Atmospheric Chemistry and Physics, 10, 11261-11276, doi:10.5194/acp-10-11261-2010, 2010.
 Qin, Y. M., Li, Y. J., Wang, H., Lee, B. P. Y. L., Huang, D. D., and Chan, C. K.: Particulate matter (PM) episodes at a suburban site in Hong Kong: evolution of PM characteristics and role of photochemistry in secondary aerosol formation, Atmospheric Chemistry and Physics, 16, 14131-14145, doi:10.5194/acp-16-14131-2016, 2016.
- Reff, A., Eberly, S. I., and Bhave, P. V.: Receptor Modeling of Ambient Particulate Matter Data Using Positive Matrix Factorization: Review of Existing Methods, Journal of the Air & Waste Management Association, 57, 146-154, doi:10.1080/10473289.2007.10465319, 2007. Rogge, W. F., Hildemann, L. M., Mazurek, M. A., and Cass, G. R.: Sources of Fine Organic Aerosol. 1. Charbroilers and Meat Cooking Operations, Environmental Science & Technology, 25, 1112-1125, 1991. Romonosky, D. E., Laskin, A., Laskin, J., and Nizkorodov, S. A.: High-resolution mass spectrometry and molecular characterization of
- 630 aqueous photochemistry products of common types of secondary organic aerosols, Journal of Physical Chemistry A, 119, 2594–2606, doi:10.1021/jp509476r, 2015.
 Rund, P., Lee, B. H., Mohr, C., and Thornton, J. A.: A Coupled Volatility and Molecular Composition Based Source Apportionment of Atmospheric Organic Aerosol, ACS Earth and Space Chemistry, 7, 1365-1377, doi:10.1021/acsearthspacechem.3c00034, 2023.
- Siemens, K. S. A., Pagonis, D., Guo, H., Schueneman, M. K., Dibb, J. E., Campuzano-Jost, P., Jimenez, J. L., and Laskin, A.: Probing Atmospheric Aerosols by Multimodal Mass Spectrometry Techniques: Revealing Aging Characteristics of Its Individual Molecular Components, ACS Earth and Space Chemistry, 7, 2498-2510, doi:10.1021/acsearthspacechem.3c00228, 2023.
 Simoneit, B. R. T.: Biomass burning a review of organic tracers for smoke from incomplete combustion, Applied Geochemistry, 17, 129-162, 2002.
- Song, J., Li, M., Jiang, B., Wei, S., Fan, X., and Peng, P. a.: Molecular Characterization of Water-Soluble Humic like Substances in Smoke Particles Emitted from Combustion of Biomass Materials and Coal Using Ultrahigh-Resolution Electrospray Ionization Fourier Transform Ion Cyclotron Resonance Mass Spectrometry, Environmental Science & Technology, 52, 2575–2585, doi:10.1021/acs.est.7b06126, 2018. Song, K., Guo, S., Gong, Y., Lv, D., Wan, Z., Zhang, Y., Fu, Z., Hu, K., and Lu, S.: Non-target scanning of organics from cooking emissions using comprehensive two-dimensional gas chromatography-mass spectrometer (GC×GC-MS), Applied Geochemistry, 151, 105601,
- 645 Song, K., Guo, S., Gong, Y., Lv, D., Zhang, Y., Wan, Z., Li, T., Zhu, W., Wang, H., Yu, Y., Tan, R., Shen, R., Lu, S., Li, S., Chen, Y., and Hu, M.: Impact of cooking style and oil on semi-volatile and intermediate volatility organic compound emissions from Chinese domestic cooking, Atmospheric Chemistry and Physics, 22, 9827-9841, doi:10.5194/acp-22-9827-2022, 2022.
 Surratt, J. D., Gómez-González, Y., Chan, A. W. H., Vermeylen, R., Shahgholi, M., Kleindienst, T. E., Edney, E. O., Offenberg, J. H.,

Lewandowski, M., Jaoui, M., Maenhaut, W., Claeys, M., Flagan, R. C., and Seinfeld, J. H.: Organosulfate Formation in Biogenic Secondary

doi:10.1016/j.apgeochem.2023.105601, 2023.

650 Organic Aerosol, The Journal of Physical Chemistry A, 112, 8345-8378, doi:10.1021/jp802310p, 2008.
Szopa, S., V. Naik, B. Adhikary, P. Artaxo, T. Berntsen, W.D. Collins, S. Fuzzi, L. Gallardo, A. Kiendler Scharr, Z. Klimont, H. Liao, Unger, N., and Zanis, P.: Short-Lived Climate Forcers. In Climate Change 2021: The Physical Science Basis. Contribution of Working Group I to the Sixth Assessment Report of the Intergovernmental Panel on Climate Change, Cambridge, United Kingdom and New York, NY, USA,, Cambridge University Press., 817–922, 10.1017/9781009157896.008, 2021.

- Thoma, M., Bachmeier, F., Gottwald, F. L., Simon, M., and Vogel, A. L.: Mass spectrometry-based Aerosolomics: a new approach to resolve sources, composition, and partitioning of secondary organic aerosol, Atmospheric Measurement Techniques, 15, 7137-7154, doi:10.5194/amt-15-7137-2022, 2022.
 - Ulbrich, I. M., Canagaratna, M. R., Zhang, Q., Worsnop, D. R., and Jimenez, J. L.: Interpretation of organic components from Positive Matrix Factorization of aerosol mass spectrometric data, Atmospheric Chemistry and Physics, 9, 2891-2918, doi:10.5194/acp-9-2891-2009, 2009
- 660 2009. Wang, Q., He, X., Huang, X. H. H., Griffith, S. M., Feng, Y., Zhang, T., Zhang, Q., Wu, D., and Yu, J. Z.: Impact of Secondary Organic Aerosol Tracers on Tracer-Based Source Apportionment of Organic Carbon and PM2.5: A Case Study in the Pearl River Delta, China, ACS Earth and Space Chemistry, 1, 562-571, doi:10.1021/acsearthspacechem.7b00088, 2017a.
- Wang, Q., Huang, X. H. H., Tam, F. C. V., Zhang, X., Liu, K. M., Yeung, C., Feng, Y., Cheng, Y. Y., Wong, Y. K., Ng, W. M., Wu, C., Chang, Q., Zhang, T., Lau, N. T., Yuan, Z., Lau, A. K. H., and Yu, J. Z.: Source apportionment of fine particulate matter in Macao, China with and without organic tracers: A comparative study using positive matrix factorization, Atmospheric Environment, 198, 183-193, doi:10.1016/j.atmosenv.2018.10.057, 2019.
 - Wang, X., Hayeck, N., Brüggemann, M., Yao, L., Chen, H., Zhang, C., Emmelin, C., Chen, J., George, C., and Wang, L.: Chemical Characteristics of Organic Aerosols in Shanghai: A Study by Ultrahigh-Performance Liquid Chromatography Coupled With Orbitrap Mass
- 670 Spectrometry, Journal of Geophysical Research: Atmospheres, 122, 11703–11722, doi:10.1002/2017jd026930, 2017b. Wang, Y., Hu, M., Lin, P., Guo, Q., Wu, Z., Li, M., Zeng, L., Song, Y., Zeng, L., Wu, Y., Guo, S., Huang, X., and He, L.: Molecular Characterization of Nitrogen-Containing Organic Compounds in Humic-like Substances Emitted from Straw Residue Burning, Environmental Science & Technology, 51, 5951-5961, doi:10.1021/acs.est.7b00248, 2017c. Wu, X., Vu, T. V., Shi, Z., Harrison, R. M., Liu, D., and Cen, K.: Characterization and source apportionment of carbonaceous PM2.5 particles
- 675 in China A review, Atmospheric Environment, 189, 187-212, doi:10.1016/j.atmosenv.2018.06.025, 2018.
 Xie, M., Chen, X., Hays, M. D., Lewandowski, M., Offenberg, J., Kleindienst, T. E., and Holder, A. L.: Light Absorption of Secondary
 - Xie, M., Chen, X., Hays, M. D., Lewandowski, M., Offenberg, J., Kleindienst, T. E., and Holder, A. L.: Light Absorption of Secondary Organic Aerosol: Composition and Contribution of Nitroaromatic Compounds, Environmental Science & Technology, 51, 11607-11616, doi:10.1021/acs.est.7b03263, 2017.
 Xu, L., Yang, Z., Tsona, N. T., Wang, X., George, C., and Du, L.: Anthropogenic-Biogenic Interactions at Night: Enhanced Formation of
- 680 Secondary Aerosols and Particulate Nitrogen- and Sulfur-Containing Organics from beta-Pinene Oxidation, Environmental Science & Technology, 55, 7794-7807, doi:10.1021/acs.est.0c07879, 2021.
 Xu, Z., Zhao, X., Li, P., Dong, Z., Sun, R., Fu, P., and Pavuluri, C. M.: Distribution and 13C Signature of Dicarboxylic Acids and Related Compounds in Fine Aerosols Near Underground Coal Fires in North China: Implications for Fossil Origin of Azelaic Acid, Journal of Geophysical Research: Atmospheres, 128, e2023JD038748, doi:10.1029/2023jd038748, 2023.
- Yao, D., Guo, H., Lyu, X., Lu, H., and Huo, Y.: Secondary organic aerosol formation at an urban background site on the coastline of South China: Precursors and aging processes, Environmental Pollution, 309, 119778, doi:10.1016/j.envpol.2022.119778, 2022.
 Yao, D., Lyu, X., Lu, H., Zeng, L., Liu, T., Chan, C. K., and Guo, H.: Characteristics, sources and evolution processes of atmospheric organic aerosols at a roadside site in Hong Kong, Atmospheric Environment, 252, 118298, doi:10.1016/j.atmosenv.2021.118298, 2021.
- Ye, J., Abbatt, J. P. D., and Chan, A. W. H.: Novel pathway of SO2 oxidation in the atmosphere: reactions with monoterpene ozonolysis intermediates and secondary organic aerosol, Atmospheric Chemistry and Physics, 18, 5549-5565, doi:10.5194/acp-18-5549-2018, 2018.

 Yu, Y., Guo, S., Wang, H., Shen, R., Zhu, W., Tan, R., Song, K., Zhang, Z., Li, S., Chen, Y., and Hu, M.: Importance of Semivolatile/Intermediate-Volatility Organic Compounds to Secondary Organic Aerosol Formation from Chinese Domestic Cooking Emissions, Environmental Science & Technology Letters, 9, 507-512, doi:10.1021/acs.estlett.2c00207, 2022.
- Yuan, Q., Zhang, Z., Chen, Y., Hui, L., Wang, M., Xia, M., Zou, Z., Wei, W., Ho, K. F., Wang, Z., Lai, S., Zhang, Y., Wang, T., and Lee,
 S.: Origin and transformation of volatile organic compounds at a regional background site in Hong Kong: Varied photochemical processes from different source regions, Science of the Total Environment, 908, 168316, doi:10.1016/j.scitotenv.2023.168316, 2024.
 Zhang, H., Yee, L. D., Lee, B. H., Curtis, M. P., Worton, D. R., Isaacman-VanWertz, G., Offenberg, J. H., Lewandowski, M., Kleindienst, T. E., Beaver, M. R., Holder, A. L., Lonneman, W. A., Docherty, K. S., Jaoui, M., Pye, H. O. T., Hu, W., Day, D. A., Campuzano-Jost, P.,
 - Jimenez, J. L., Guo, H., Weber, R. J., de Gouw, J., Koss, A. R., Edgerton, E. S., Brune, W., Mohr, C., Lopez-Hilfiker, F. D., Lutz, A., 00 Kreisberg, N. M., Spielman, S. R., Hering, S. V., Wilson, K. R., Thornton, J. A., and Goldstein, A. H.: Monoterpenes are the largest source of summertime organic aerosol in the southeastern United States, Proceedings of the National Academy of Sciences of the United States of America, 115, 2038-2043, doi:10.1073/pnas.1717513115, 2018.
 - Zhang, M., Cai, D., Lin, J., Liu, Z., Li, M., Wang, Y., and Chen, J.: Molecular characterization of atmospheric organic aerosols in typical megacities in China, npj Climate and Atmospheric Science, 7, 230, doi:10.1038/s41612-024-00784-1, 2024.
- 705 Zhang, Y., Men, Y., Guo, H., Shen, G., Gao, Y., Xiong, R., Tao, S., and Wang, X.: Combustion-related isoprene contributes substantially to the formation of wintertime secondary organic aerosols, National Science Review, 12, nwae474, doi:10.1093/nsr/nwae474, 2025.Zhang, Y., Peräkylä, O., Yan, C., Heikkinen, L., Äijälä, M., Daellenbach, K. R., Zha, Q., Riva, M., Garmash, O., Junninen, H., Paatero, P., Worsnop, D., and Ehn, M.: A novel approach for simple statistical analysis of high-resolution mass spectra, Atmospheric Measurement Techniques, 12, 3761-3776, doi:10.5194/amt-12-3761-2019, 2019.

- 710 Zheng, P., Chen, Y., Wang, Z., Liu, Y., Pu, W., Yu, C., Xia, M., Xu, Y., Guo, J., Guo, Y., Tian, L., Qiao, X., Huang, D. D., Yan, C., Nie, W., Worsnop, D. R., Lee, S., and Wang, T.: Molecular Characterization of Oxygenated Organic Molecules and Their Dominating Roles in Particle Growth in Hong Kong, Environmental Science & Technology, 57, 7764-7776, doi:10.1021/acs.est.2c09252, 2023. Zhou, W., Xu, W., Kim, H., Zhang, Q., Fu, P., Worsnop, D. R., and Sun, Y.: A review of aerosol chemistry in Asia: insights from aerosol mass spectrometer measurements, Environmental Science Processes & Impacts, 22, 1616-1653, doi:10.1039/d0em00212g, 2020.
- 715 Zhu, M., Jiang, B., Li, S., Yu, Q., Yu, X., Zhang, Y., Bi, X., Yu, J., George, C., Yu, Z., and Wang, X.: Organosulfur Compounds Formed from Heterogeneous Reaction between SO2 and Particulate-Bound Unsaturated Fatty Acids in Ambient Air, Environmental Science & Technology Letters, 6, 318-322, doi:10.1021/acs.estlett.9b00218, 2019.
 Zhu, T., Tang, M., Gao, M., Bi, X., Cao, J., Che, H., Chen, J., Ding, A., Fu, P., Gao, J., Gao, Y., Ge, M., Ge, X., Han, Z., He, H., Huang, R.-J., Huang, X., Liao, H., Liu, C., Liu, H., Liu, J., Liu, S. C., Lu, K., Ma, Q., Nie, W., Shao, M., Song, Y., Sun, Y., Tang, X., Wang, T.,
- 720 Wang, T., Wang, W., Wang, X., Wang, Z., Yin, Y., Zhang, Q., Zhang, W., Zhang, Y., Zhang, Y.,

Supplement of

Molecular Insights into Organic Aerosol Sources and Formation at a Regional Background Site in South China Hongxing Jiang et al.,

730 Correspondence to: H. Guo (hai.guo@polyu.edu.hk)

The copyright of individual parts of the supplement might differ from the article licence.

Supplementary text

HR-TOF-AMS analysis

lockdown, at Hok Tsui, a regional background site in Hong Kong, to study the influence of transport from mainland China on local air quality. During this period, we employed an online high-resolution time-of-flight aerosol mass spectrometer (HR-TOF-AMS, Aerodyne Inc.) to measure the chemical composition of NR-PM₁, including total organics, sulfate, nitrate, ammonium, and chloride. The AMS alternated between V-mode and W-mode on a 2-minute cycle. Elemental composition of organics was determined using W-mode data, which provides high mass resolution (~5000-6000), and was subsequently used for OA source apportionment. To ensure the accuracy of NR-PM₁ measurements, the instruments were regularly calibrated with pure chemical standards, such as ammonium nitrate, both before and during the sampling period. Pure ammonium nitrate particles (350nm in diameter) were applied to calibrate the ionization efficiency (IE) for m/z 30 and m/z 46. Based on weekly calibrations, the relative ionization efficiency (RIE) value for ammonium was determined to be 4.0. In addition, particle 745 velocity during sampling was calibrated using Nanosphere PSL particles of various sizes (50, 100, 200, 300, 400, 500, and 600nm; Duke Scientific, Palo Alto, CA, USA). The collection efficiency (CE) of NR-PM₁ was determined by comparing AMS NR-PM1 measurements with PM1 concentrations measured by HKEPD, after subtracting black carbon at the same location. PM1 and black carbon concentrations from HKEPD were obtained using a Tapered Element Oscillating Microbalance (TEOM) and a black carbon analyzer (BC, model AE16, Magee, USA), respectively. The final CE value for this study was determined to be 0.73 and was applied to all measured NR-PM₁ components. Finally, the collection efficiency (CE) for this study was determined to be 0.73 and was applied to all measured NR-PM₁ components. Data processing was performed using the ToF-AMS Analysis Toolkit 1.59D and TofAMS HR Analysis 1.19D, both implemented in Igor Pro 6.37 software. RIEs of 1.4, 1.1, 1.2, 4.0, and 1.3 were applied for total organics, nitrate, sulfate, ammonium and chloride, respectively. Method detection limits (MDLs) for each species were determined by collecting background mass spectra (HEPA filtered air, 60 min every 2 days). The calculated MDLs wer 0.21µg m⁻³ for organics, 0.020 μg m⁻³ for nitrate, 0.022μg m⁻³ for sulfate, 0.013 μg m⁻³ for ammonium, and 0.013 μg m⁻³ for chloride. OA source apportionment was conducted using the Positive Matrix Factorization (PMF) Evaluation Toolkit (PET v2.05). To ensure robust results, several steps were followed as described in our previous studies, including the application of minimum error values and ion filtration (Huo et al., 2024a; Yao et al., 2022). The optimal 4-factor solution was selected based on O/O_{exp} values, residuals, and mass spectra(Zhang et al., 2011). Figure. S1 presents the mass spectra of the 4 OA factors resolved by $PMF. \ The \ HOA \ factor \ was \ characterized \ by \ abundant \ alkyl \ fragments \ (C_nH_{2n+1}^+ \ and \ C_nH_{2n-1}^+), \ such \ as \ C_3H_7^+, \ C_4H_7^+, \ C_4H_7^+,$ and C₄H₉⁺ (Sun et al., 2011). In this study, the HOA factor had O/C and H/C values of 0.25 and 1.72, respectively, the lowest and highest among the 4 factors. Notably, the O/C value was higher than typical ranges for HOA reported in previous studies (e.g., 0.05-0.25), indicating the influence of atmospheric aging (Huo et al., 2024a). The other 3 factors exhibited high loadings of oxygenated species, such as m/z 44 (mainly CO₂⁺), confirming their classification as oxygenated OA components. These 3

We conducted a comprehensive sampling campaign in autumn 2020 (September 29 to November 18), during the COVID-19

OOA factors were divided into two less oxidized OOAs (LO-OOA1 and LO-OOA2) and one more oxidized OOA (MO-OOA) based on their O/C values. The LO-OOA factors also contained many alkyl fragments, indicating a closer association with primary sources.

TAG-EI-TOF-MS analysis

During the sampling period, TAG-EI-TOF-AMS analysis was used to quantify SOA tracers in the particle phase. Detailed descriptions of the instrument and its performance are available in our previous studies (Huo et al., 2024b; Lyu et al., 2020). Briefly, air samples were collected using a collection and thermal desorption (CTD) unit at 30 °C with a flow rate of 10 L min⁻¹ over 90 min. Derivatization occurred in the CTD unit by purging it with a mixed flow of pure helium (20 mL/min) and saturated N-methyl-N-(trimethylsilyl) trifluoroacetamide (MSTFA)-helium (80 mL/min). The CTD unit was heated to 315 °C over 9 minutes and held at that temperature for 5 minutes, allowing derivatives to be desorbed and transferred to a focusing trap (FT) unit (~30 °C), where target compounds and their derivatives were trapped while excess MSTFA and most volatile organics were vented. The FT was then gradually heated to 315 °C over 12 minutes, with pure helium purging the target compounds from the FT to a mini-gas chromatography (GC) column. The GC column was operated under a programmed temperature profile (0.75 mL/min), starting at ~40 °C and increasing to 45 °C in 1 minute, then rapidly rising to 330 °C over 10 minutes, and held at 330 °C for 12 minutes until the end of the GC analysis. Before sampling, external standards with known concentrations were used for identification and quantification of target compounds. To address desensitization and peak drift during analysis, a mixture of 26 deuterated internal compounds with constant concentrations was injected alongside each sample. In total 62 compounds were identified, with details provided in Table S2.

PTR-TOF-MS analysis

An online proton transfer reaction quadrupole ion time-of-flight mass spectrometer (PTR-TOF-MS, IONICON Analytik GmbH, Innsbruck, Austria) was used to measure concentrations of VOC species. Detailed information about the instrument is available in previous studies (Yuan et al., 2024). Ambient air was continuously drawn at a rate of 3.0 L/min through a Teflon tube equipped with a 4.7 mm Teflon-membrane filter (Whatman Ihc. Clifton, NJ, USA). A small fraction of this air (0.2 L/min) was introduced into the TOF-MS for VOCs measurements. Certified standard gas mixtures (1 ppm, Linde Spectra Environmental Gases, USA) were used to quantify target VOCs species, determine the instrument's transmission curve, and assess sensitivities. The PTR-TOF-MS was calibrated weekly at room temperature using a liquid calibration unit (LCU, Ionicon).

Other ancillary measurements

In addition to the online instruments used for detecting atmospheric organics, a suite of other online instruments was employed to measure concentrations of PM_{2.5}, trace gases (CO, NO, NO₂, O₃ and SO₂), and meteorological parameters (temperature and relative humidity). PM_{2.5} concentrations were measured using a Tapered Element Oscillating Microbalance (TEOM) (Thermo ScientificTM 1405). SO₂ concentrations were determined with a Teledyne Advanced Pollution Instrumentation (API) Trace-

level UV Fluorescence SO₂ Analyzer (T100U), while nitrogen species were measured using the Teledyne True NO₂/NO/NO_x Analyzer (T200UP) Ozone (O₃) concentrations were measured With an Ecotech UV Absorption Ozone Analyzer (EC9810B/S10). The photolysis frequency of NO₂ (*J*NO₂) was measured using a MetCon Filter Radiometer.

Carbon analysis

805

830

The concentrations of organic carbon (OC) and elemental carbon (EC) in $PM_{2.5}$ were determined using a Sunset OC/EC analyzer with an enhanced thermal/optical reflectance protocol. A 1.5 cm² section of each $PM_{2.5}$ filter was placed in a quartz boat and subjected to stepwise heating in a quartz furnace to separate OC and EC. During analysis, four OC peaks (OC1, OC2, OC3, and OC4) and three EC peaks (EC1, EC2, and EC3) were identified. Pyrolyzed organic carbon (PyC), formed by the coking of OC during the procedure, was monitored through changes in laser reflectance signals. The total OC and EC contents were calculated using the formulas as follows: OC = OC1 + OC2 + OC3 + OC4+ PyC; EC= EC1 + EC2 + EC3-PyC.

HR-orbitrap-MS analysis

The molecular composition of OAs in offline PM_{2.5} filters was analyzed using a high-resolution Q-Executive Orbitrap mass spectrometer (Thermo Electron, Inc.) coupled with an ultra-high performance liquid chromatography system (UHPLC, Dionex UltiMate 3,000, Thermo Electron, Inc.). Detailed descriptions of the analysis procedures and instrumental settings are available in a previous study (Zhang et al., 2024). Briefly, two pieces of PM_{2.5} filters were punched using a stainless-steel puncher (Φ=20 mm), and the dissolved organic matter was extracted with 6 mL of mix-solvents (2×3 times, methanol: toluene=1:1, v/v) in an ultrasonic cold-water bath for 20 minutes. The extracts were filtered through a 0.22 μm polytetrafluoroethylene filter membrane, combined, and evaporated to near dryness under a gentle stream of high-purity nitrogen. The residue was then redissolved in 150 μL of methanol and centrifuged, with the supernatant transferred for subsequent HR-MS analysis.

As noted in previous studies, potential intermolecular suppression effects can occur during the ionization process (Zhang et al., 2024; Thoma et al., 2022). To address these challenges, a UHPLC system was employed for compound separation. Samples (5 μL) were injected into the system, and separation was performed on an Acquity UPLC HSS T3 column (1.8 μm particle size, 100 mm × 2.1 mm; Waters, Milford, MA, USA) with a VanGuard pre-column (HSS T3, 1.8 μm) at a flow rate of 0.3 mL min⁻¹. A gradient elution procedure was used for compounds isolation, with eluent A/B consisting of 0.1% formic acid in ultrapure water/methanol. Eluent B was initially maintained at 10% for 2 min, increased to 54% over 15.2 min and held for 1 min, then increased to 90% over 7.5 min and held for 0.2 min, before returning to 1% within 1.8 min and held for 9.6 min before the next sample. Analytes were introduced to the heated electrospray ionization (ESI) source system and ionized in negative mode. The spray voltages were set as 3.0 kV for ESI–, with the capillary temperature at 320°C. The sheath gas flow, auxiliary gas flow, and sweep gas flow were set 35, 10, and 0 units, respectively. The mass spectrometer scanned a range of m/z 50-800 with a typical mass resolution of 140,000 at m/z 200.

Xcalibur software (V2.2; Thermo Scientific) was used to acquire raw data, while further non-target compound analysis was performed using the open-source MZmine-2.37 software (http://mzmine.github.io). This analysis included raw data import, peak detection, shoulder peak filtering, chromatogram building, chromatogram deconvolution, deisotoping, searching for

adducts and peak complexes, alignment, gap filling, identification, and duplicate peak filtering. Detailed processing steps and settings are described in previous literature (Wang et al., 2017). Mass peaks were assigned to specific molecules with a mass tolerance of 2 ppm for ESI- mode. The atoms in the assigned molecular formulas were limited to $C_{1-40}H_{0-100}O_{0-40}N_{0-5}S_{0-3}$, with additional criteria on elemental ratios (e.g., H/C, O/C) and double bond equivalents (DBE) applied to eliminate chemically meaningless molecular formulas. The elemental ratios, DBE, and modified aromatic index were calculated based on the assigned formulas of $C_cH_hO_oN_nS_s$, where c, h, o, n, and s represent the number of carbon, hydrogen, oxygen, nitrogen, and sulfur atoms, respectively. All molecules reported in this study underwent blank subtraction, and those with an abundance ratio of less than 5:1 were eliminated (Ditto et al., 2018).

835

The chemical parameters, including DBE, nO_{eff} , (Nie et al., 2022), AI_{mod} (Koch and Dittmar, 2006), and volatility (LogC*) 840 (Li et al., 2016), of the compounds are calculated using the following equations respectively:

$$\begin{split} \text{DBE} &= (2 \ n_C + 2 - \ n_H + n_N)/2 \\ nO_{\text{eff}} &= n_O - 2 \ n_N - 3 \ n_S \\ \text{AI} &= (1 + n_C - 0.5 n_O - n_S - 0.5 n_H)/(\ n_C - 0.5 n_O - n_S - n_N) \\ Log_{10}C^* &= (n_C^0 - n_C)b_C - n_Ob_O - 2 \frac{n_C n_O}{n_C + n_O}b_{CO} - n_Nb_N - n_Sb_S \end{split}$$

where n_C , n_H , n_O , n_N , and n_S denote the numbers of carbon, hydrogen, oxygen, nitrogen, and sulfur atoms in the molecular formula, respectively. n_C^0 is the reference carbon number. The parameters b_C , b_O , b_N , and b_S denote the contribution of each atom to $log_{10}C^*$, respectively, while b_{CO} is the carbon–oxygen nonideality.

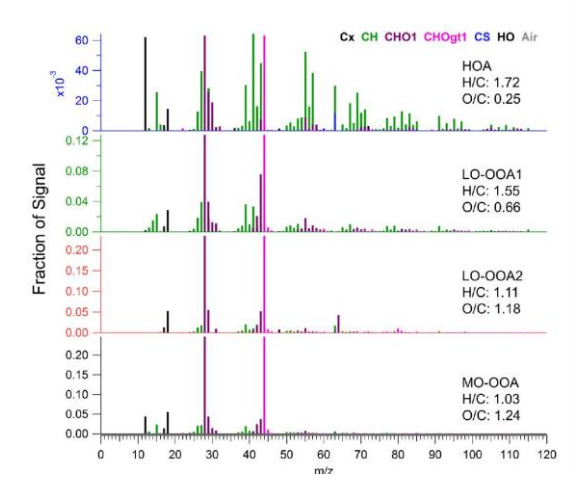


Figure S1. Mass spectra of OA components obtained from AMS-PMF analysis

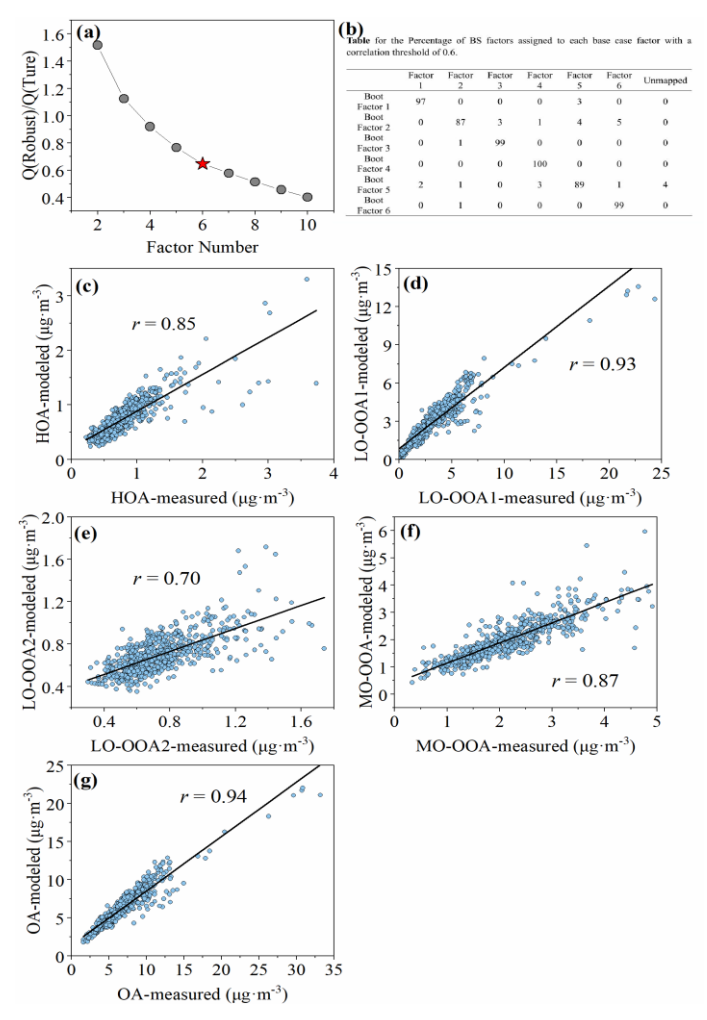


Figure S2. Diagnostic results for tracer-based PMF analysis. (a) Variation of average Q/Q_{exp} with increasing number of factors in PMF. (b) Table showing the percentage of bootstrap (BS) factors assigned to each base case factor, using a correlation threshold of 0.6. (c-g) Correlation analysis between the concentrations of AMS-PMF derived OA components and the tracer-based PMF modeled values

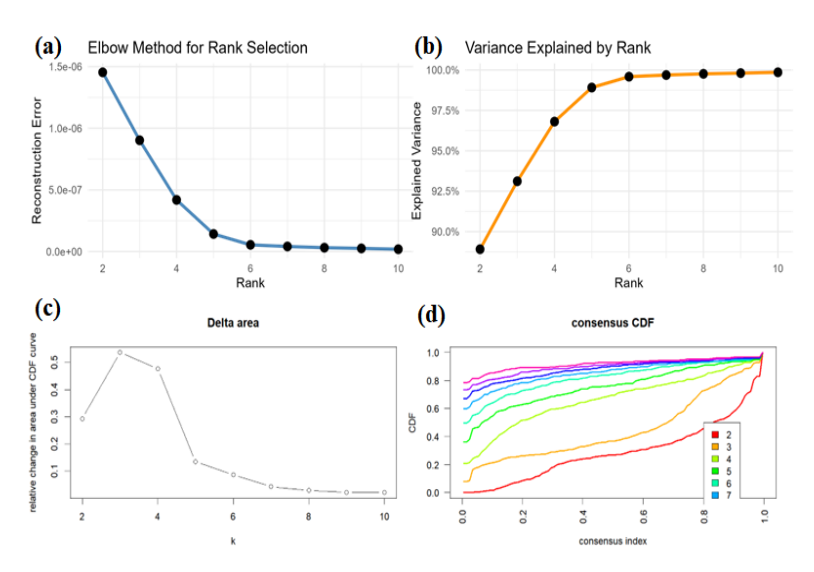


Figure S3. Diagnostic results for PMF results-constrained NMF analysis. (a) Variation of re-constructured error with increasing number of factorss. (b) Variation of explained total variances with increasing number of factors. and (c) Variation of the cumulative distribution function (CDF) delta area with increasing number of factors. (d) Cumulative distribution functions of the consensus matrix for each factor number, estimated using a histogram with 100 bins

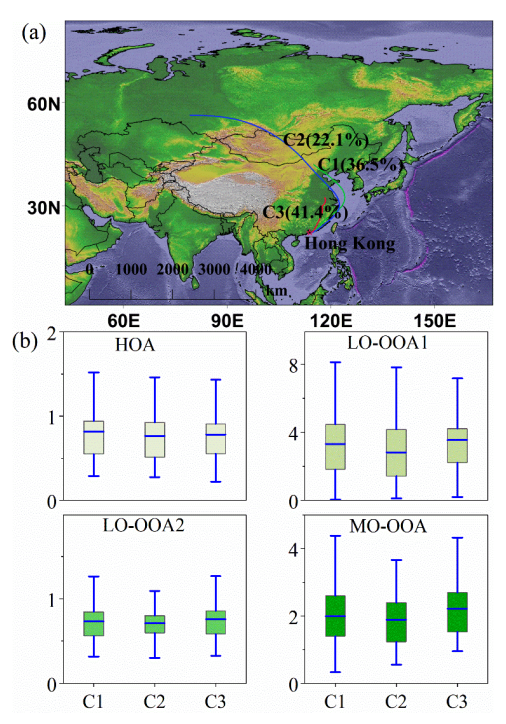


Figure S4. (a) Air mass clusters based on 120-hr backward trajectories arriving at the sampling site during the study period. (b) Box plots of the four OA components for different air mass influence periods. In each box, the blue line denotes the mean value, the upper (lower) boundary of the box represents the 75th (25th) percentile, and the top and bottom whiskers indicate the 95th and 5th percentiles, respectively.

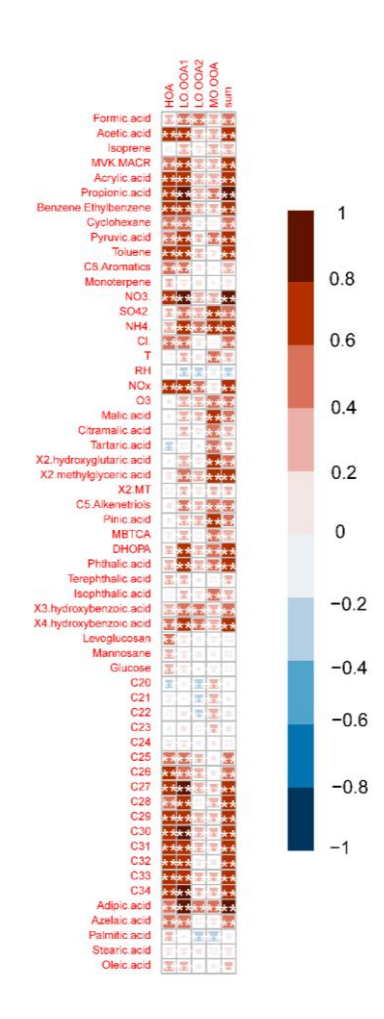


Figure S5. Correlations between AMS-PMF derived OA components and selected chemical species.

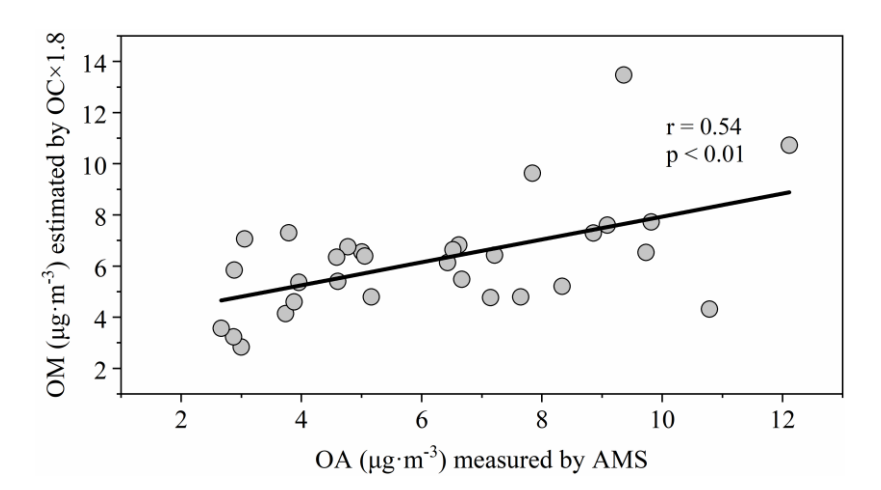


Figure S6. Correlations between AMS-derived OA concentrations and estimated OM (OC multiplied by a factor of 1.8). The
observed correlation coefficient suggests that, despite uncertainties in OM estimation, potential discrepancies between AMS
and OC/EC analyzer measurements, and the limited sample size, OA in PM₁ likely shares similar sources and formation
pathways with OM in PM_{2.5}.

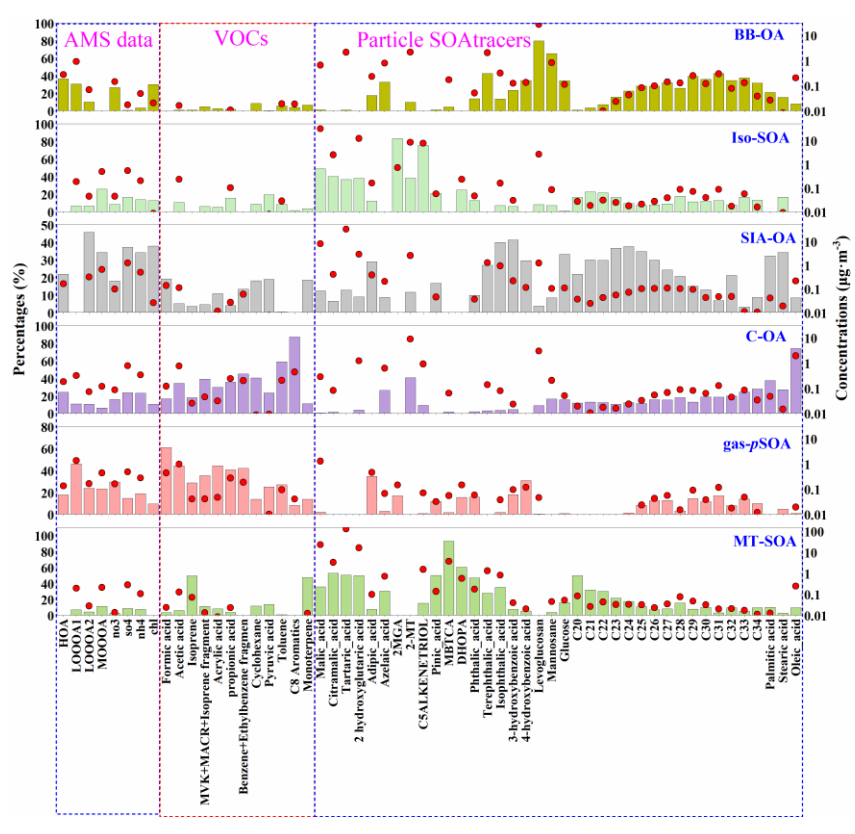


Figure S7. Source profiles of individual factors identified in the 6-factor solution resolved by tracer-based PMF.

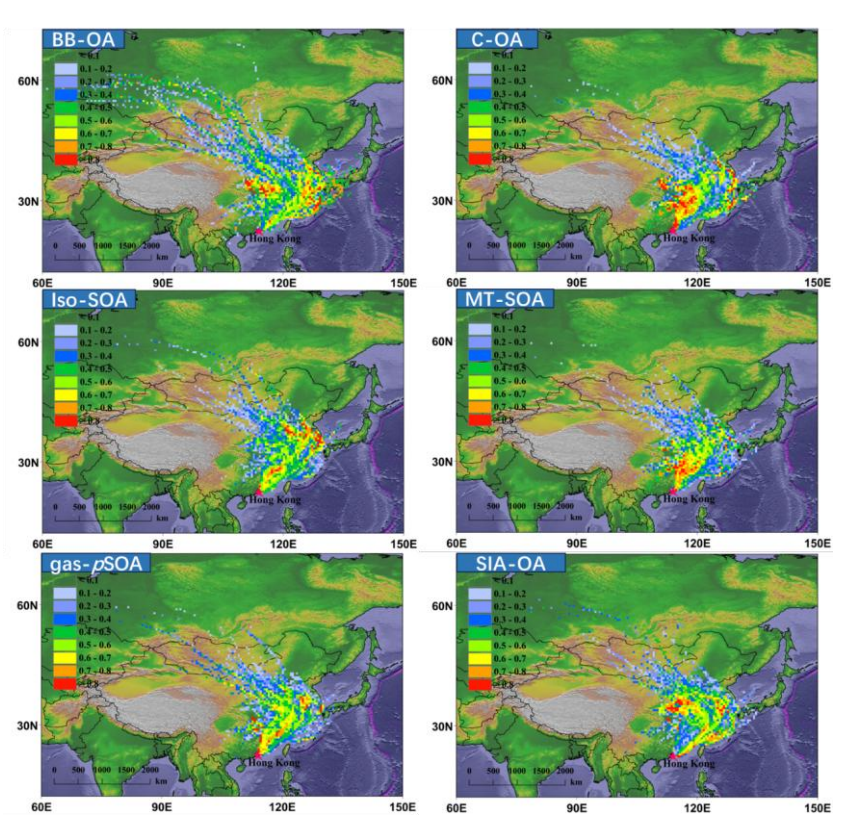


Figure S8. PSCF maps of the 6 PMF-resolved sources during the sampling period. The color gradient denotes the potential source contributions.

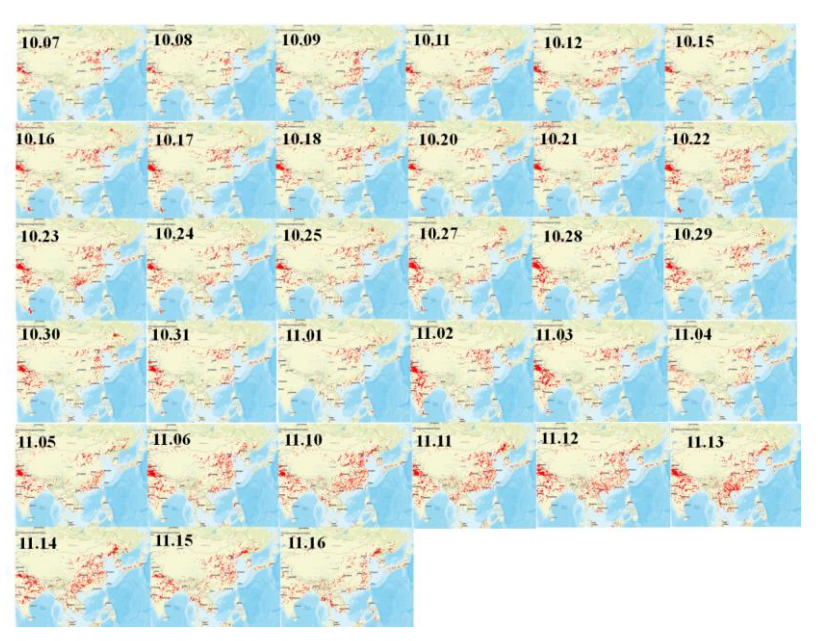


Figure S9. Daily fire maps corresponding to the offline $PM_{2.5}$ filter sampling dates.

设置了格式: 下标

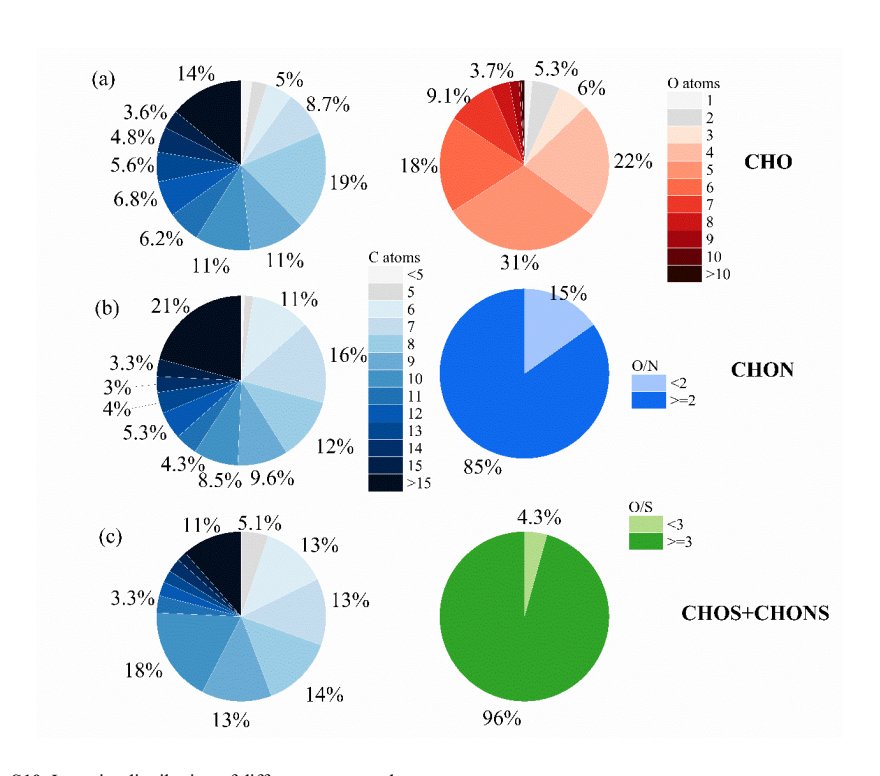


Figure S10. Intensity distribution of different compound groups

880

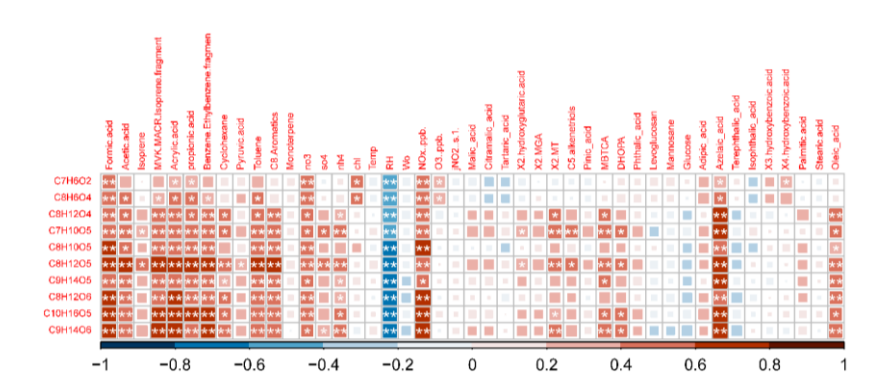


Figure S11. Correlations between the intensities of several highly abundant CHO compounds and selected chemical species.

Table S1. Sampling information for offline PM_{2.5} samples.

Sampling ID	Sampling	PM _{2.5}	Temp (°C)	RH (%)	OC (μg·m ⁻	EC (μg·m ⁻
	date	$(\mu g\!\cdot\! m^{\text{-}3})$			3)	3)
HT01	2020/10/07	16.4	24.3	72	5.41	1.63
HT02	2020/10/08	16.8	25.0	68	5.05	1.60
HT03	2020/10/09	22.0	25.6	68	6.73	2.10
HT04	2020/10/10	13.8	26.7	76	4.92	1.97
HT05	2020/10/11	13.5	26.6	82	4.36	1.13
HT06	2020/10/12	14.5	25.9	77	5.99	2.56
HT07	2020/10/15	17.0	25.7	78	4.63	1.31
HT08	2020/10/16	16.0	24.6	77	4.25	1.26
HT09	2020/10/17	14.8	24.0	77	3.97	1.31
HT10	2020/10/18	18.3	23.4	70	2.56	1.27
HT11	2020/10/19	21.0	24.4	62	2.78	1.16
HT12	2020/10/20	16.0	25.6	61	2.87	0.96
HT13	2020/10/21	20.8	23.5	54	3.70	1.19
HT14	2020/10/22	23.2	23.5	70	5.45	1.04
HT15	2020/10/23	13.0	24.2	76	1.70	0.55
HT16	2020/10/24	11.4	24.0	81	1.67	0.60
HT17	2020/10/25	10.7	23.3	84	1.60	0.59

设置了格式: 下标

HT18	2020/10/27	19.7	23.9	84	2.11	1.19	
HT19	2020/10/28	20.2	23.5	76	2.81	0.86	
HT20	2020/10/29	12.5	23.2	72	2.08	0.76	
HT21	2020/10/30	20.9	23.9	72	2.65	0.95	
HT22	2020/10/31	26.7	23.5	67	3.57	1.45	
HT23	2020/11/01	26.8	23.3	69	4.01	1.35	
HT24	2020/11/02	16.6	24.2	60	2.15	0.83	
HT25	2020/11/03	11.7	22.8	77	1.48	0.74	
HT26	2020/11/04	34.8	26.1	59	5.20	2.05	
HT27	2020/11/05	22.0	22.4	66	3.68	1.18	
HT28	2020/11/06	16.4	21.7	67	2.20	0.71	
HT29	2020/11/10	19.4	22.6	68	3.62	1.43	
HT30	2020/11/11	21.3	22.0	80	2.55	1.03	
HT31	2020/11/13	19.0	23.0	77	1.60	0.61	

885

 Table S2. Quantified compounds identified using TAG-EI-TOF-MS.

Compounds	Abbreviations	IS
Malic acid	MA	¹³ C-Pentaerythritol
Citramalic acid	CA	¹³ C-Pentaerythritol
Tartaric acids	TA	¹³ C-Pentaerythritol
2-hydroxyglutaric acid	2-HGA	¹³ C-Pentaerythritol
2-methylglyceric acid	2-MGA	¹³ C-Pentaerythritol
cis-2-methyl-1,3,4trihydroxy-1-butene		¹³ C-Pentaerythritol
3-methyl-2,3,4trihydroxy-1-butene	C5-alkenetriols	¹³ C-Pentaerythritol
trans-2-methy-1,3,4trihydroxy-1-butene		¹³ C-Pentaerythritol
2-methylthreitol	A 3 477	¹³ C-Pentaerythritol
2-methylerythritol	2-MTs	¹³ C-Pentaerythritol
Pinic acid	PA	1-Dodecan-D25-ol
3-methyl-1,2,3butanetricarboxylic acid	MBTCA	¹³ C-Pentaerythritol
2,3-dihydroxy-4oxopentanoic acid	DHOPA	¹³ C-Pentaerythritol
Phthalic acid	PhA	D-phthalic acid
Terephthalic acid	TPA	D-phthalic acid
Isophthalic acid	IPA	D-Pentadecanol
Levoglucosan	Lev	¹³ C-Pentaerythritol
Mannosane	Man	¹³ C-Pentaerythritol
Glucose	Glu	¹³ C-Pentaerythritol
Adipic acid	AdiA	D-adipic acid
Azelaic acid	AzeA	D-Pentadecanol
3-hydroxybenzoic acid	3-HBA	1-Dodecan-d25-ol
4-hydroxybenzoic acid	4-HBA	1-Dodecan-d25-ol
Palmitic acid	PalA	1-Octadeca-d37-nol
Stearic acid	StA	Stearic-d35 acid
Oleic acid	OleA	Stearic-d35 acid
C20		Eicosane-d42
C21		Eicosane-d42
C22		Docosane-d46
C23		Docosane-d46
C24		Tetracosane-d50
C25		Tetracosane-d50
C26		Hexacosane-d54
C27		Hexacosane-d54

Octacosane-d58	C28
Octacosane-d58	C29
Triacontane-d62	C30
Triacontane-d62	C31
Dotriacontane-d66	C32
Dotriacontane-d66	C33
Tetratriacontane-d70	C34

Table S3. Most intense compounds detected within wach compound group.

Formula	MW	DBE	AI_{mod}	VOC class	Structural	Possible name or Precursors
			CHC	compound	ds	Trecursors
C ₆ H ₁₀ O ₁	98.19	2	0.27	VOC	Lipids	Fatty acids (Sun et al., 2011)
$C_7H_6O_2$	122.17	5	0.67	IVOC	CRAMS	Benzoic acid and hydroxybenzaldehyde
$C_7H_{10}O_2$	126.20	3	0.33	IVOC	CRAMS	Trimethyl benzene isomers (Mehra et al., 2020)
$C_7H_{10}O_4$	158.20	3	0.20	IVOC	CRAMS	Trimethyl benzene isomers (Mehra et al., 2020)
$C_8H_6O_4$	166.19	6	0.67	IVOC	CRAMS	Phthalic acid
C ₈ H ₁₂ O ₄	172.24	3	0.17	IVOC	CRAMS	cis-Norpinic acid/ terpenylic acid
C ₇ H ₁₀ O ₅	174.20	3	0.11	IVOC	HOC	Bicyclic hydroperoxide
C ₈ H ₁₄ O ₄	174.25	2	0.00	IVOC	Protein	Suberic acid
C ₇ H ₁₂ O ₅	176.22	2	0.00	IVOC	Carbohydrates	Monoterpenes
C ₈ H ₆ O ₅	182.19	6	0.64	IVOC	CRAMS	Hydroxyphthalic acid
$C_8H_{10}O_5$	186.22	4	0.27	IVOC	CRAMS	Trimethyl benzene isomers/ monoterpenes
C ₉ H ₁₄ O ₄	186.27	3	0.14	IVOC	Protein	Pinic acid
C ₈ H ₁₂ O ₅	188.23	3	0.09	IVOC	CRAMS	Monoterpene / hydroxyterpenylic acid
C ₉ H ₁₆ O ₄	188.29	2	0.00	IVOC	Protein	Azelaic acid / monoterpene
$C_8H_{14}O_5$	190.25	2	0.00	IVOC	Protein	Diaterpenylic acid/ monoterpene
C ₉ H ₁₂ O ₅	200.25	4	0.23	IVOC	CRAMS	Aromatics (Molteni et al., 2018)
$C_8H_{10}O_6$	202.22	4	0.20	SVOC	НОС	Trimethyl benzene isomers/ isoprene (Nguyen et al., 2011)
C ₉ H ₁₄ O ₅	202.27	3	0.08	IVOC	Protein	Monoterpene

C ₈ H ₁₂ O ₆	204.23	3	0.00	SVOC	HOC	Monoterpene/
						Trimethylbenzene
$C_{10}H_{14}O_5$	214.29	4	0.20	IVOC	CRAMS	Monoterpene
C ₁₀ H ₁₆ O ₅	216.30	3	0.07	IVOC	Protein	Monoterpene
C ₉ H ₁₄ O ₆	218.27	3	0.00	SVOC	Protein	Monoterpene/
C911 ₁₄ O ₆	210.27	3	0.00	5100	Trotein	Trimethylbenzene
C ₁₂ H ₁₄ O ₄	222.32	6	0.40	IVOC	CRAMS	Monoterpene/biomass
C121114O4	222.32	Ü	0.40	1000	CICAIVIS	burning
$C_{10}H_{14}O_6$	230.29	4	0.14	SVOC	CRAMS	Monoterpene
$C_{11}H_{18}O_5$	230.34	3	0.06	SVOC	Protein	Monoterpene
$C_{10}H_{16}O_{6}$	232.30	3	0.00	SVOC	Protein	Monoterpene
$C_{12}H_{18}O_5$	242.35	4	0.16	SVOC	CRAMS	Monoterpene
$C_{11}H_{16}O_6$	244.32	4	0.13	SVOC	CRAMS	Biogenic
$C_{12}H_{20}O_5$	244.37	3	0.05	SVOC	Protein	Biogenic
$C_{13}H_{20}O_5$	256.39	4	0.14	SVOC	Protein	β-Caryophyllene
			СНО	N compoun	ds	
C ₆ H ₅ NO ₃	139.15	5	0.86	IVOC	CRAMS	Nitrophenol/catechol
C ₅ H ₄ N ₂ O ₃	140.13	5	1.67	IVOC	CRAMS	Methylglyoxal
						+Ammonium Sulfate
C ₇ H ₇ NO ₃	153.19	5	0.67	IVOC	CRAMS	Nitrocresol
C ₆ H ₅ NO ₄	155.15	5	0.83	IVOC	CRAMS	4-Nitrocatechol
$C_8H_6N_2O_2$	162.20	7	1.00	SVOC	CRAMS	3-Nitroindole
C ₇ H ₄ N ₂ O ₃	164.17	7	1.29	SVOC	Condensed	
					Aromatics	\
C ₈ H ₇ NO ₃	165.20	6	0.73	IVOC	CRAMS	Nitroacetophenone or
						methyl-
						nitrobenzaldehyde
C ₈ H ₉ NO ₃	167.22	5	0.55	IVOC	CRAMS	Dimethyl-nitrophenol
C ₇ H ₇ NO ₄	169.18	5	0.63	SVOC	CRAMS	2-Methyl-4-
						nitroresorcinol
C ₇ H ₅ NO ₅	183.17	6	0.86	SVOC	HOC	2-Methyl-5-
						nitrobenzoic acid
C ₉ H ₁₇ NO ₃	187.30	2	0.00	SVOC	Protein	Biomass burning
C ₁₀ H ₇ NO ₃	189.24	8	0.80	SVOC	CRAMS	2-Nitro-1-naphthol
C ₉ H ₇ NO ₄	193.22	7	0.75	SVOC	CRAMS	Biomass burning

$C_8H_7NO_5$	197.20	6	0.67	SVOC	CRAMS	Methyl-hydroxy-
						nitrobenzoate
C ₈ H ₉ NO ₅	199.22	5	0.44	SVOC	CRAMS	Dimethoxy-nitrophenol
C ₇ H ₄ N ₂ O ₇	228.17	7	1.67	LVOC	Others	Toluene/ 3,5-
						dinitrosalicylic acid
C ₆ H ₃ N ₃ O ₇	229.15	7	0.00	LVOC	Others	Picric acid
C ₂₃ H ₁₇ N ₃ O ₂	367.56	17	0.76	ELVOC	Unsaturated	\
					Hydrocarbons	1
C ₂₃ H ₄₉ NO ₄	403.80	0	0.00	LVOC	Others	\
C ₂₇ H ₁₇ N ₅ O ₁₆	667.64	22	0.82	ULVOC	Condensed	\
					Aromatics	1
-		(CHOS+C	HONS com	pounds	
$C_6H_{10}O_6S_1$	210.25	2	0	SVOC	Others	Green leaf volatiles
C ₆ H ₁₂ O ₆ S ₁	212.26	1	0	SVOC	Others	Monoterpene/ olefinic
						acid
C ₅ H ₁₀ O ₇ S ₁	214.23	1	0	LVOC	Others	Isoprene/ olefinic acid
C ₇ H ₁₂ O ₆ S ₁	224.28	2	0	SVOC	Carbohydrates	Monoterpene
C ₆ H ₁₀ O ₇ S ₁	226.25	2	0	LVOC	Others	Isoprene/ green leaf
						volatiles
C ₇ H ₁₄ O ₆ S ₁	226.30	1	0	SVOC	Carbohydrates	Olefinic acid
C ₆ H ₁₂ O ₇ S ₁	228.26	1	0	LVOC	Others	Isoprene
C ₇ H ₁₂ O ₇ S ₁	240.28	2	0	LVOC	Others	Isoprene
C ₆ H ₁₀ O ₈ S ₁	242.25	2	0	LVOC	Others	\
C ₉ H ₁₆ O ₆ S ₁	252.35	2	0	SVOC	Protein	Monoterpene
C ₈ H ₁₄ O ₇ S ₁	254.32	2	0	LVOC	Carbohydrates	Monoterpene
C ₇ H ₁₂ O ₈ S ₁	256.28	2	0	LVOC	Others	Isoprene
C ₈ H ₁₂ O ₈ S ₁	268.30	3	0	LVOC	HOC	Monoterpene
C ₁₀ H ₁₆ O ₇ S ₁	280.37	3	0	LVOC	Carbohydrates	Monoterpene
C ₉ H ₁₄ O ₈ S ₁	282.33	3	0	LVOC	Carbohydrates	Monoterpene
C ₁₀ H ₁₈ O ₇ S ₁	282.38	2	0	LVOC	Carbohydrates	Monoterpene
C ₈ H ₁₂ O ₉ S ₁	284.30	3	0	LVOC	Others	\
C ₉ H ₁₆ O ₈ S ₁	284.35	2	0	LVOC	Carbohydrates	Monoterpene
$C_{10}H_{17}O_7N_1S_1$	295.38	3	0	ELVOC	Carbohydrates	Monoterpene
$C_{10}H_{16}O_8S_1$	296.37	3	0	LVOC	Carbohydrates	Monoterpene
					*	

Table S4. Intensity-weighted molecular characteristics of organic compounds associated with NMF-derived OA factors

	CookingC-	IsopreneSOA <u>Iso-</u>	Biomass	Gasgas-	SIA-OA _{NMF}
	<u>OA</u> NMF	SOA _{NMF}	burningB-	p SOA $_{NMF}$	
			<u>OA</u> _{NMF}	_	
MW	216	213	217	221	214
C	8.91	9.44	10.00	9.25	9.76
Н	12.75	13.38	12.92	12.78	13.76
O	5.25	5.02	4.81	5.42	4.83
N	0.22	0.11	0.33	0.20	0.17
S	0.28	0.12	0.07	0.23	0.10
H/C	1.44	1.42	1.28	1.38	1.40
O/C	0.63	0.59	0.52	0.63	0.56
N/C	0.03	0.01	0.04	0.03	0.02
S/C	0.04	0.01	0.01	0.03	0.01
O/N	0.88	0.30	1.09	0.71	0.40
O/S	1.84	0.75	0.43	1.59	0.56
N/S	0.09	0.04	0.03	0.04	0.03
DBE	3.64	3.81	4.71	3.96	3.97
DBE/C	0.41	0.42	0.49	0.44	0.43
nO_{eff}	3.97	4.43	3.94	4.34	4.18
$\mathrm{AI}_{\mathrm{mod}}$	0.20	0.22	0.34	0.24	0.24
Xc	1.40	1.28	1.70	1.46	1.40
LogC*	1.42	2.12	1.90	1.39	2.09
		Compounds c	lasses		
DBE=0	0.68	1.76	0.30	0.65	1.2
DBE=1	5.8	4.6	4.0	4.8	3.9
DBE=2	19	17	13	18	14
DBE=3	29	28	22	25	22
DBE>=4	45	49	61	51	58
Condensed	3.7	3.3	5.6	3.0	3.1
Aromatics					
CRAMS	36	34	43	36	38
Lipids-like	4.7	7.4	10.6	6.1	9.1
Protein-like	18	25	20	21	19
HOC	12	11	10	12	13
Carbohydrates-	12	5	4	8	2
<u>like</u>					

设置了格式: 下标 设置了格式: 字体: 倾斜

Unsaturated	0.88	1.25	0.72	0.56	2.7
Hydrocarbons					
Others	13	14	5	13	13

References

- Ditto, J. C., Barnes, E. B., Khare, P., Takeuchi, M., Joo, T., Bui, A. A. T., Lee-Taylor, J., Eris, G., Chen, Y., Aumont, B., Jimenez, J. L., Ng, N. L., Griffin, R. J., and Gentner, D. R.: An omnipresent diversity and variability in the chemical composition of atmospheric functionalized organic aerosol, Communications Chemistry, 1, 75, doi:10.1038/s42004-018-0074-3, 2018.
- Huo, Y., Yao, D., and Guo, H.: Differences in aerosol chemistry at a regional background site in Hong Kong before and during the COVID-19 pandemic, Sci Total Environ, 926, 171990, doi:10.1016/j.scitotenv.2024.171990, 2024a. Huo, Y., Lyu, X., Yao, D., Zhou, B., Yuan, Q., Lee, S. c., and Guo, H.: Exploring the Formation of High Levels of Hydroxyl Dicarboxylic Acids at an Urban Background Site in South China, Journal of Geophysical Research: Atmospheres, 129,

e2023JD040096, doi:10.1029/2023jd040096, 2024b.

Koch, B. P. and Dittmar, T.: From mass to structure: an aromaticity index for high-resolution mass data of natural organic matter, Rapid Communications in Mass Spectrometry, 20, 926-932, doi:10.1002/rcm.2386, 2006. Li, Y., Poschl, U., and Shiraiwa, M.: Molecular corridors and parameterizations of volatility in the chemical evolution of

organic aerosols, Atmospheric Chemistry and Physics, 16, 3327-3344, doi:10.5194/acp-16-3327-2016, 2016.

- Lyu, X., Guo, H., Yao, D., Lu, H., Huo, Y., Xu, W., Kreisberg, N., Goldstein, A. H., Jayne, J., Worsnop, D., Tan, Y., Lee, S. C., and Wang, T.: In Situ Measurements of Molecular Markers Facilitate Understanding of Dynamic Sources of Atmospheric Organic Aerosols, Environ Sci Technol, 54, 11058-11069, doi:10.1021/acs.est.0c02277, 2020. Mehra, A., Wang, Y., Krechmer, J. E., Lambe, A., Majluf, F., Morris, M. A., Priestley, M., Bannan, T. J., Bryant, D. J., Pereira,
- K. L., Hamilton, J. F., Rickard, A. R., Newland, M. J., Stark, H., Croteau, P., Jayne, J. T., Worsnop, D. R., Canagaratna, M. 20 R., Wang, L., and Coe, H.: Evaluation of the chemical composition of gas- and particle-phase products of aromatic oxidation,
 - Atmospheric Chemistry and Physics, 20, 9783-9803, doi:10.5194/acp-20-9783-2020, 2020. Molteni, U., Bianchi, F., Klein, F., El Haddad, I., Frege, C., Rossi, M. J., Dommen, J., and Baltensperger, U.: Formation of highly oxygenated organic molecules from aromatic compounds, Atmospheric Chemistry and Physics, 18, 1909-1921, doi:10.5194/acp-18-1909-2018, 2018.
- Nguyen, T. B., Roach, P. J., Laskin, J., Laskin, A., and Nizkorodov, S. A.: Effect of humidity on the composition of isoprene photooxidation secondary organic aerosol, Atmospheric Chemistry and Physics, 11, 6931-6944, doi:10.5194/acp-11-6931-
 - Nie, W., Yan, C., Huang, D. D., Wang, Z., Liu, Y., Qiao, X., Guo, Y., Tian, L., Zheng, P., Xu, Z., Li, Y., Xu, Z., Qi, X., Sun, P., Wang, J., Zheng, F., Li, X., Yin, R., Dallenbach, K. R., Bianchi, F., Petäjä, T., Zhang, Y., Wang, M., Schervish, M., Wang,
- S., Qiao, L., Wang, Q., Zhou, M., Wang, H., Yu, C., Yao, D., Guo, H., Ye, P., Lee, S., Li, Y. J., Liu, Y., Chi, X., Kerminen, V.-M., Ehn, M., Donahue, N. M., Wang, T., Huang, C., Kulmala, M., Worsnop, D., Jiang, J., and Ding, A.: Secondary organic aerosol formed by condensing anthropogenic vapours over China's megacities, Nature Geoscience, 15, 255-261, doi:10.1038/s41561-022-00922-5, 2022.
- Sun, Y. L., Zhang, Q., Schwab, J. J., Demerjian, K. L., Chen, W. N., Bae, M. S., Hung, H. M., Hogrefe, O., Frank, B., Rattigan, O. V., and Lin, Y. C.: Characterization of the sources and processes of organic and inorganic aerosols in New York city with a high-resolution time-of-flight aerosol mass apectrometer, Atmospheric Chemistry and Physics, 11, 1581-1602, doi:10.5194/acp-11-1581-2011, 2011.
 - Thoma, M., Bachmeier, F., Gottwald, F. L., Simon, M., and Vogel, A. L.: Mass spectrometry-based Aerosolomics: a new approach to resolve sources, composition, and partitioning of secondary organic aerosol, Atmospheric Measurement Techniques, 15, 7137-7154, doi:10.5194/amt-15-7137-2022, 2022.
- Wang, X., Hayeck, N., Brüggemann, M., Yao, L., Chen, H., Zhang, C., Emmelin, C., Chen, J., George, C., and Wang, L.: Chemical Characteristics of Organic Aerosols in Shanghai: A Study by Ultrahigh-Performance Liquid Chromatography Coupled With Orbitrap Mass Spectrometry, J. Geophys. Res. Atmos., 122, 11703–11722, doi:10.1002/2017jd026930, 2017. Yao, D., Guo, H., Lyu, X., Lu, H., and Huo, Y.: Secondary organic aerosol formation at an urban background site on the
- coastline of South China: Precursors and aging processes, Environmental Pollution, 309, 119778, doi:10.1016/j.envpol.2022.119778, 2022.

Yuan, Q., Zhang, Z., Chen, Y., Hui, L., Wang, M., Xia, M., Zou, Z., Wei, W., Ho, K. F., Wang, Z., Lai, S., Zhang, Y., Wang, T., and Lee, S.: Origin and transformation of volatile organic compounds at a regional background site in Hong Kong: Varied photochemical processes from different source regions, Sci Total Environ, 908, 168316, doi:10.1016/j.scitotenv.2023.168316, 2024.

Zhang, M., Cai, D., Lin, J., Liu, Z., Li, M., Wang, Y., and Chen, J.: Molecular characterization of atmospheric organic aerosols in typical megacities in China, npj Climate and Atmospheric Science, 7, 230, doi:10.1038/s41612-024-00784-1, 2024.

Zhang, Q., Jimenez, J. L., Canagaratna, M. R., Ulbrich, I. M., Ng, N. L., Worsnop, D. R., and Sun, Y.: Understanding atmospheric organic aerosols via factor analysis of aerosol mass spectrometry: a review, Anal Bioanal Chem, 401, 3045-3067, doi:10.1007/s00216-011-5355-y, 2011.